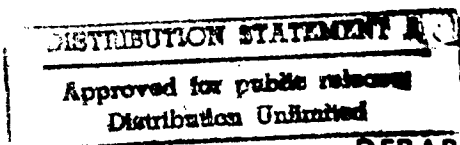THE DESIGN AND DEVELOPMENT OF A LOW-
SPEED, LOW-FORCE WIND TUNNEL DATA
ACQUISITION SYSTEM WITH AN APPLICATION
TO BICYCLE FRONT FORK SPACING

THESIS

Alan W. Elledge, Captain, USAF

AFIT/GAE/ENY/94D-21

DEPARTMENT OF THE AIR FORCE

AIR UNIVERSITY

AIR FORCE INSTITUTE OF TECHNOLOGY

Wright-Patterson Air Force Base, Ohio

AFIT/GAE/ENY/94D-21

THE DESIGN AND DEVELOPMENT OF A LOW-
SPEED, LOW-FORCE WIND TUNNEL DATA
ACQUISITION SYSTEM WITH AN APPLICATION
TO BICYCLE FRONT FORK SPACING

THESIS

Alan W. Elledge, Captain, USAF

AFIT/GAE/ENY/94D-21

The views expressed in this thesis are those of the author and do not reflect the official policy or position of the Department of Defense or the U.S. Government.

THE DESIGN AND DEVELOPMENT OF A LOW-SPEED. LOW-FORCE

WIND TUNNEL DATA ACQUISITION SYSTEM WITH AN APPLICATION

TO BICYCLE FRONT FORK SPACING

THESIS

Presented to the Faculty of the School of Engineering

of the Air Force Institute of Technology

Air University

In Partial Fulfillment of the

Requirements for the Degree of

Master of Science in Aeronautical Engineering

Alan W. Elledge, B.S.

Captain, USAF

December 1994

Preface

The United States Cycling Federation is working with the United States Olympic Committee to develop the most technologically advanced and aerodynamic bicycle, or 'superbike,' for the 1996 Olympics. The USCF approached Wright Laboratory in hopes that the Air Force would provide resources to assist them in their quest. In turn, Wright Laboratory contacted AFIT with the intent of finding a Master's student to provide support to the program.

It would have been hard to imagine the Air Force conducting bicycle research a few years ago. However, in today's world of cooperation, sharing, and joint projects between government and private industry, technology transition is fast becoming a way of life and good business practice. But the project would also benefit the Air Force in terms of future research capabilities.

The AFIT 5-ft Wind Tunnel was built in the 1920's. It was built to research aerodynamics and test the most technologically advanced aircraft of the era. One of the inspectors for the tunnel was none other than Orville Wright. It almost seemed a bit ironic that the latest use of the tunnel was for the aerodynamics of bicycles.

This project was immense. It was more than a full time job starting at the end of the spring quarter and running all the way up until the last minute at the end of November. I would only be partly finished with the project if it was not for my partner, Capt Brian Parker. His support throughout the project was indispensable. He provided support, insight, and encouragement throughout the project. I am forever grateful for his efforts and participation in the project. Although our projects were closely related, they were indeed separate. Brian's main area of contribution was in the design of the flexures used for the cylinder and bicycle. We both worked on the tunnel's low-speed capabilities and cylinder data. My individual efforts were the data acquisition system design and construction and, of course, the front fork spacing investigation.

In addition, I would like to thank everyone in the model fabrication shop for all their hard work in supporting us on the project. They all contributed to the success. And even for a time in October, their support in producing the last pieces of equipment for the project demonstrated their dedication to the students at AFIT.

And what can I say about Charles McNealy? He truly gave 100% to the project. I often thought he was dedicated to working only on our project. His support and tireless efforts were greatly appreciated.

But wait, there are more. I would like to thank the thesis committee members, Dr. Paul King, Dr. Phil Beran, and most of all, my thesis advisor, Dr. Milton Franke. His encouragement and enthusiasm during the project kept us going when it looked like we would never finish.

But all of these thank you's are only secondary to that which I give to my wife, Gena. Her support, understanding, and patience, all while being pregnant, gave me the strength to see this project through. Her positive attitude, helpfulness, and cheer all made the effort worthwhile, and at times, fun.

<div align="right">Alan W. Elledge</div>

Table of Contents

List of Tables

List of Symbols and Acronyms

AOA	angle of attack
ASCII	American Standard Code for Information Interchange
axfor	axial force
b	intercept
c	tunnel cross section area
C_d	drag coefficient
C_{di}	induced drag coefficient
C_l	lift coefficient
D	drag
D_b	buoyancy drag
dl	change in the jet length
dp	change in static pressure
DNL	Digital Noise Level
E_{in}	bridge input excitation voltages
E_{zero}	zero point bridge input excitation voltages
$Error_{force}$	root sum square error of drag force
$Error_{RSS}$	root sum square error
k	body shape factor modified for tunnel test section shape
LSB	least significant bit
LSBrms	least significant bit (root mean squared)
m	slope
s	model reference area

q	tunnel dynamic pressure
qcorr	corrected tunnel dynamic pressure
USCF	United States Cycling Federation
USOC	United States Olympic Committee
V	volts
V_{out}	strain gage output voltage
V_{zero}	zero point strain gage output voltage
VDC	volts direct current
vol	model volume
Δ	change in
Δu_i	uncertainty of a parameter
Ω	ohms
$\dfrac{\partial s}{\partial u}$	sensitivity due to a parameter

Abstract

This thesis encompassed the design, development, and application of a low-speed, low-force data acquisition system for the AFIT 5-ft Wind Tunnel. The new data acquisition system was designed and developed to measure approximately 0.045 N (about 0.01 lb_f) at nearly 64.4 km/h (40 mph). Verification of the capability was obtained through testing of a cylindrical model. As part of a technology transition program with Wright Laboratory, this new system was used to investigate bicycle front fork blade spacing in order to determine the optimal spacing for minimum drag. As for the minimum drag of a bicycle with an adjustable-width front fork, the spacing should be kept to a minimum.

The wind tunnel was deemed to have sufficiently smooth and steady flow for conducting low-speed research at or above 29 km/h (18 mph), the minimum tunnel velocity using the rear set of motors with the flow straightener positioned directly in front of the inlet.

Chapter 1. Introduction

The testing of various objects at low speeds often involves sensitive measurement equipment and adequate testing facilities. Since the AFIT 5-ft Wind Tunnel was not designed for such tests, its low-speed capabilities were investigated. In addition, since the aerodynamic drag of a bicycle traveling at 48 km/h is only 10.7 N, the ability to detect small changes in drag was also developed. These requirements were made in the light of Huffy Corporation's tests performed in the same wind tunnel during 1985. Those tests involved various aerodynamic bicycles for the 1988 Olympics. However, the data was inconclusive because of inaccuracies and coarse measurements resulting from the spring balances and weights in use at the time.

1. Background

Bicycle racing is important to America. Although mostly a European sport, it has spread in recent years to the United States through the start of organized racing in cities such as Pittsburgh and Los Angeles. Even some long distance American road races such as the former Coors Classic and the increasingly popular Tour Du Pont have attracted some international legends of the sport, including some American favorites such as Greg LeMond and Lance Armstrong.

Bicycle racing, both road and track, is a highly competitive sport. In the semifinal team pursuit race during this years' world track cycling championship in Palermo, Italy, the U.S. team beat the Australian team by a mere 0.027 seconds ("Whipping World", 1994:16). And in the world of road racing, the 1994 Tour of Mexico (14 stages covering a total of 1759 km (1093 miles)) was won by 22 seconds (Kita, 1994:16). And who can forget the 1989 Tour de France in which Greg LeMond came from 50 seconds behind at the start of the final 24.1 km (15 mile) time trial to defeat Laurent Fignon by 8 seconds (Kyle, 1989:24). What is amazing is that by reducing

the aerodynamic drag by minuscule amounts, the outcomes of these races could have been reversed (see Table 1).

Table 1. The Racing Advantage of Aerodynamic Drag Reduction

Decrease in Drag (N)	Time Difference (s/km)	Lead Distance (m/km)	Savings for 1000m Time Trial (s)	Savings for 4000m Pursuit Race (s)
0.098	0.07	0.95	0.07	0.28
0.196	0.14	1.90	0.12	0.62
0.392	0.28	3.80	0.23	1.12
0.785	0.58	7.80	0.47	2.22
1.177	0.86	11.6	0.70	3.39
1.961	1.56	21.0	1.17	5.62
				Taken from (Kyle, 1991b:394)

What makes this so amazing is aerodynamic drag. Next to the rider's ability, the most influential factor affecting the race is aerodynamic drag. Over 90% of the retarding force at racing speeds (over 32.2 km/h (20 mph)) is due to the wind from the bicycle's speed (Kyle and Burke, 1984:36; Hopkins and Principe, 1990:5; Kyle, 1989:24). According to Kyle and Burke, (1984:36), there are four ways to reduce wind resistance: lowering the projected frontal area, streamlining, smoothing corners and roughnesses, and relocating non-aerodynamic shapes. The single best way to make improvements is by altering rider position. The next best alternative is to improve the aerodynamics of the bike and its components.

One might make an argument for lighter equipment or riders in order to reduce racing times. Reducing the weight translates to less inertia. Since rapid acceleration and deceleration are important and quite frequent in a racing situation, the effect is multiplied. Although reducing the weight will indeed reduce race times, that is not the best way to reduce racing times (Kyle and

Burke. 1984:43; Kyle. 1991a:29). From Table 2, one can deduce that the reductions in time per newton of added weight fall far short of those achieved through aerodynamic reductions (see Table 1).

Table 2. Effect of Adding Weight to Individual Race Times

Weight Added to 801 N (180 lb$_f$)	Time added for 1000 m	Time added for 4000 m
4.4 (1.0)	0.03 s	0.01 s
8.9 (2.0)	0.05 s	0.04 s
17.8 (4.0)	0.08 s	0.09 s
Taken from (Kyle and Burke, 1984:44)		

Several advances in recent years have drastically reduced the drag on a bicycle. Table 3 shows some typical results of aerodynamic changes.

Table 3. Drag Reduction Comparison at 48 km/h

Item	Drag N (lb$_f$)	Time Saved over 24.1 km (15 mi)
standard track bike (no rider)	10.63 (2.39)	-
aero bike (2.4 to 1 tubing) (no rider)	6.23 (1.4)	1.2 min
standard track bike (with rider)	35.90 (8.07)	-
aero bike (2.4 to 1 tubing) (with rider)	34.34 (7.72)	25 s
std water bottle	0.89 (0.2)	-
aero water bottle	0.76 (0.17)	2.1 s
Laurent Fignon's pony tail	0.49 (0.11)	8 s
Laurent Fignon's lack of aero helmet use	1.38 (0.31)	22 s
Difference between LeMond and Fignon	6.01 (1.35)	1.30 min
Taken from (Kyle and Burke, 1984:41; Kyle, 1989: 24)		

Although the many improvements made to the bicycle have drastically improved the racing times, recent events still show that a 0.05 N savings in aerodynamic drag can mean the difference between a win or a loss. Winning a race by a tire length can equate to only 0.1 N of aerodynamic drag (Kyle, 1990:27).

One area of drag reduction not given much attention is the area of the front fork (see Figure 1). Typically, front forks are comprised of a steerer tube, crown, and two blades running down from the crown to the front wheel axle. An obvious reduction in drag would come from
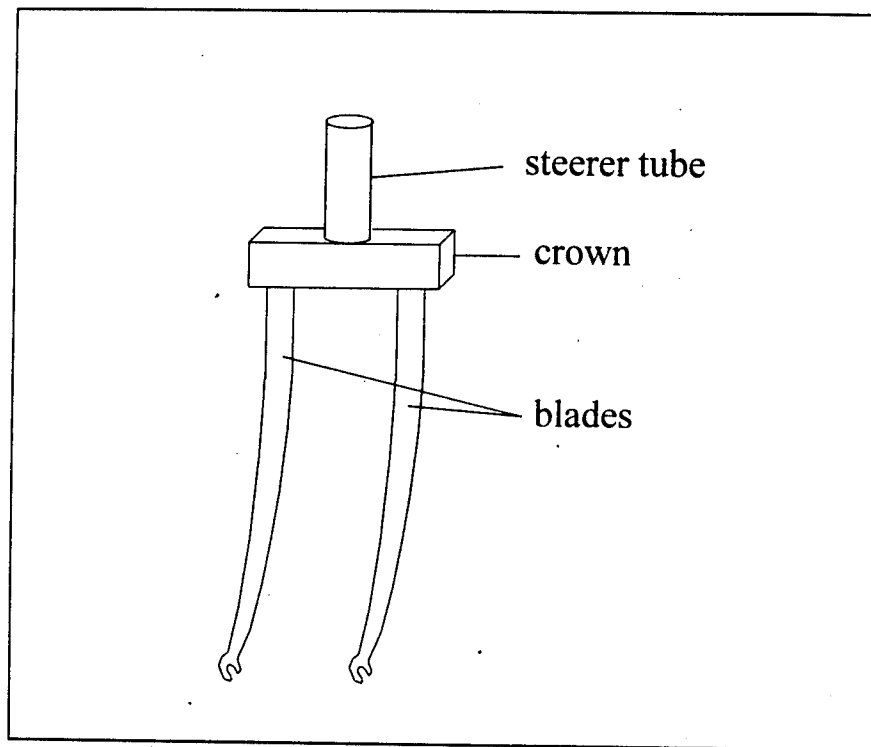
Figure 1. Components of a Typical Bicycle Front Fork

aerodynamic shaping of the blades. In addition, reducing drag through the use of a monoblade fork has been studied. However, little research has been done in studying the effect of spacing between the blades and the wheel. It was therefore likely that a spacing for minimum drag existed. This project was designed to determine that optimum spacing.

This problem is not as simple as positioning two stationary objects relative to each other to determine the minimum drag configuration. Numerous non-traditional factors affect the drag relationship. First, and probably foremost, is the effect of the spinning wheels. As the bicycle wheels spin, they impart a velocity to the surrounding air because of the no-slip boundary condition. Since the top of the wheel moves "upstream" relative to the wind velocity, the imparted velocity is opposite to the freestream. It is this influence that complicates the drag reduction. Additional factors affecting the drag include the spokes and the shapes of all the fork and wheel components.

When one considers the physical size of the fork and wheel interaction region with respect to the entire bicycle, its contribution to the overall drag of the bicycle seems minimal, but even the slightest decrease in aerodynamic drag saves time in any race. This alone helps to give the rider an advantage. More importantly, changes made to the position of the fork blades with respect to the wheel normally would not affect the rider or rider's position. Without any biomechanical changes required because of altered fork spacing, the rider can still use his normal and efficient riding position.

2. Problem Statement

Several previous studies and wind tunnel tests identified numerous ways to reduce bicycle drag; however, there may be some additional reduction available due to fork blade spacing. Therefore, this study investigated the spacing of bicycle front forks in order to determine the

optimal spacing for minimum drag. In order to measure small changes in drag on the order of 0.05-0.1 N, wind tunnel capabilities were assessed and an accurate measurement device and technique were developed and verified.

3. Facilities

This investigation was conducted in the AFIT 5-ft Wind Tunnel located in Building 19 of Area B, Wright-Patterson AFB, OH. The test section is 1.5m (5 ft) in diameter. Tunnel air flow is generated from two sets of two motors. Each motor set drives a set of 3.7 m (12 ft) diameter, counterrotating fan blades. The front set of blades is located approximately 15.2 m (50 ft) from the trailing edge of the test section and the rear set is located approximately 22.9 m (75 ft) from the test section. Although only one set of motors was needed to generate the low speeds required for testing, tunnel velocities reaching nearly 322 km/h (200 mph) can be obtained with both sets of motors operating. The Reynolds number for the bicycle tests ranged from 6.0×10^4 to 1.5×10^5 per meter, well below the maximum of 6.2×10^6 per meter. The tunnel has a movable flow straightener located at the inlet. The straightener is capable of being moved nearly 3.0 m (10 ft) away from the inlet of the tunnel.

Since the tunnel is an open-circuit, continuous type, the total pressure for the tunnel is atmospheric. Static pressure measurements are obtained through a ring of 8 static pressure ports located 0.76 m (2.5 ft) from the tunnel mouth and 3.4 m (11 ft) upstream of the test section. The ports are arranged in a ring and the average static pressure was obtained as recommended by Rae and Pope (1984:143). Dynamic pressure is obtained from the difference between the total pressure and the average of the static pressure ports. The two fans, flow straightener, and tunnel wall vibrations all contribute to the test section turbulence factor of 1.5.

4. Phases

This investigation involved several small, but significant, steps in leading up to the investigation of bicycle front fork blade spacing. Because of the significance of each, the project was broken down into four phases. Phase I consists of a wind tunnel low-speed capability assessment. Phase II details the vertical sting and data acquisition system design and development. Phase III follows with a verification of the data system and low-force, low-speed capability by measuring and comparing true drag of a three-dimensional cylinder. And finally, the application of the system to determine the optimal spacing of a bicycle front fork for the least amount of drag is covered in Phase IV. Each of these phases is described in terms of key characteristics such as scope, equipment, test set-up, and data analysis.

Chapter 2. Phase I - Wind Tunnel Low-Speed Capability

In order to accomplish the objective of studying fork spacing, the wind tunnel was operated in the very low speed range (32-64 km/h (20-40 mph)) and it was necessary for the test section air flow outside the boundary layer had to be fairly uniform and relatively free of turbulence (Rae and Pope, 1984:73). Although a rigorous study of the flow quality was out of the scope of this experiment, some investigation of the flow quality was desired.

1. Scope

An extensive study of the tunnel flow quality using pressure rakes throughout the test section exceeded the scope of this phase. However, both qualitative and quantitative data were gathered to gain a simple, yet adequate, assessment of flow uniformity and level of turbulence. The first test, a flow visualization test (Section 2.3) provided a qualitative assessment of the flow over the ground plane. Section 4 highlights the static pressure test, a quantitative test used to show flow steadiness through the tunnel's test section. And finally for Section 5, the tunnel dynamic pressure was monitored while various tunnel parameters were varied. This last test also determined the best configuration for low-speed tunnel operation.

2. Equipment

Several pieces of equipment, including a ground plane, pressure measurement system, and dynamic pressure measurement system, were required for this phase. Each piece is described.

2.1. Pressure measurement system

Pressure System Inc. supplied the Model 780B/T Pressure Measurement System used to collect pressure data. The system was composed of Electronically Scanned Pressure (ESP) sensors

and a microcomputer-based data acquisition system. The overall accuracy of the system was maintained by frequent, user-transparent, on-line calibrations of the transducers. The on-line calibration, accurate to ±0.1% full scale, used a three-point calibration which employed a quartz pressure transducer. The system was capable of acquiring 20k measurements per second. The electronic scanner used was the Pressure Systems Electronic Pressure Scanner, Model ESP-32, with a range of ±6895 Pa (±1 psid). Therefore, the accuracy of the pressure measurements was ±6.9 Pa (±0.001 psid).

2.2. Dynamic pressure system

As previously mentioned, the tunnel dynamic pressure was determined by the difference between 8 averaged static pressures and atmospheric pressure. The model 11234 transducer used for the static pressure was manufactured by Statham. Maximum pressure for the transducer was 103.4 kPa (15 psig) at 11 VDC. The accuracy of the transducer was ±1034 Pa (±0.15 psid).

2.3. Ground plane

In order to simulate ground effects, a ground plane was used for the bicycle tests. Although a moving ground plane with rotating wheels would be more realistic (Rae and Pope, 1984:418) for proper simulation of a bicycle moving over stationary ground in calm conditions (i.e. no boundary layer on the ground), practicality prohibited it. Thus, a 1.9 m (6 ft-2 in) long by 0.64 m (25 in) wide, stationary ground plane, made of 1.9 cm (0.75 in) thick plywood, was fabricated and installed with the leading edge 3.0 m (10 ft) from the inlet of the tunnel. Air flow under the ground plane was unrestricted while the centerline clearance above the plane was nearly 1.49 m (58 in) (see Figure 2). This mounting height helped reduce the size of the boundary layer over the ground plane as no suction device was used to remove the boundary layer from the ground plane.
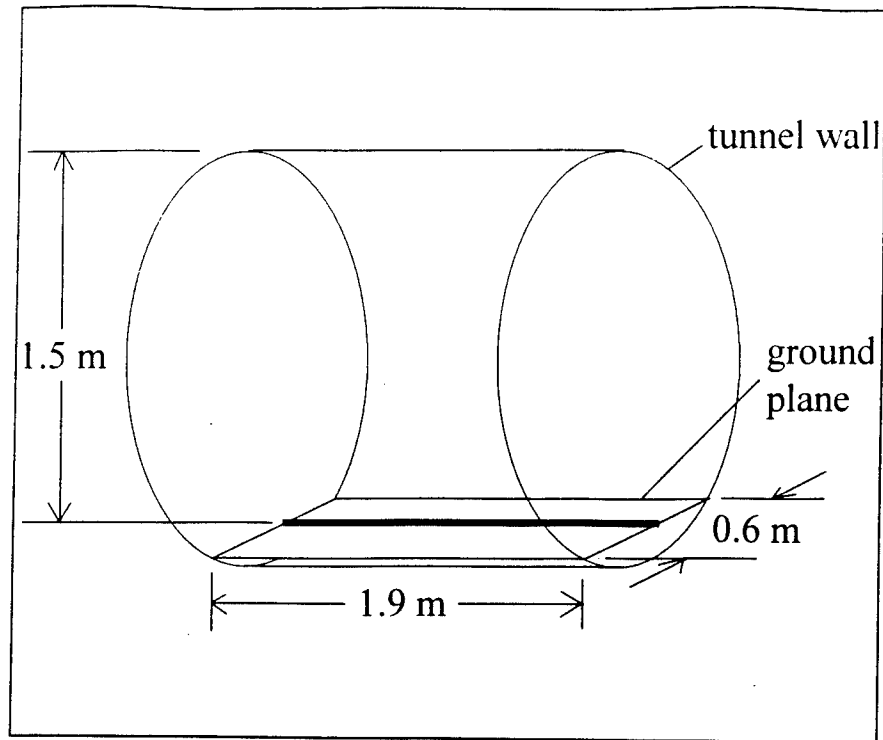
Figure 2. Ground Plane Configuration

The plane was covered with a smooth laminate and marked with a painted centerline to aid in model alignment. The leading edge of the ground plane was shallowly beveled on the lower surface. This bevel helped prevent the blunt surface from causing separated flow. It also kept flow skewing effects to a minimum. The trailing edge was left square.

3. Flow Quality - Tufts

The flow quality over the ground plane was observed with tufts installed at several stations. The leading and trailing edges were more densely tufted than the middle section. Tufts were about 3.8 cm (1.5 in) long, made from needlepoint thread, and secured with cellophane tape.

Visual observations were made as wind speeds varied from 32 to 64 km/h (20 to 40 mph). The first runs were made with a protective metal guard on the leading edge of the ground plane.

Most of the tufts exhibited a minimal amount of fluttering at all speeds (see Figure 3). A few tufts, especially along one side of the leading edge, displayed some flow reversal (see Figure 4). This was attributed to the metal guard and imperfections and other anomalies in the tunnel walls near the leading edge of the ground plane. Additional runs made without the guard in place displayed virtually no flow reversal or fluttering. Therefore, the flow over the ground plane was determined to be of good quality with the metal guard removed. Future runs were conducted without the guard.
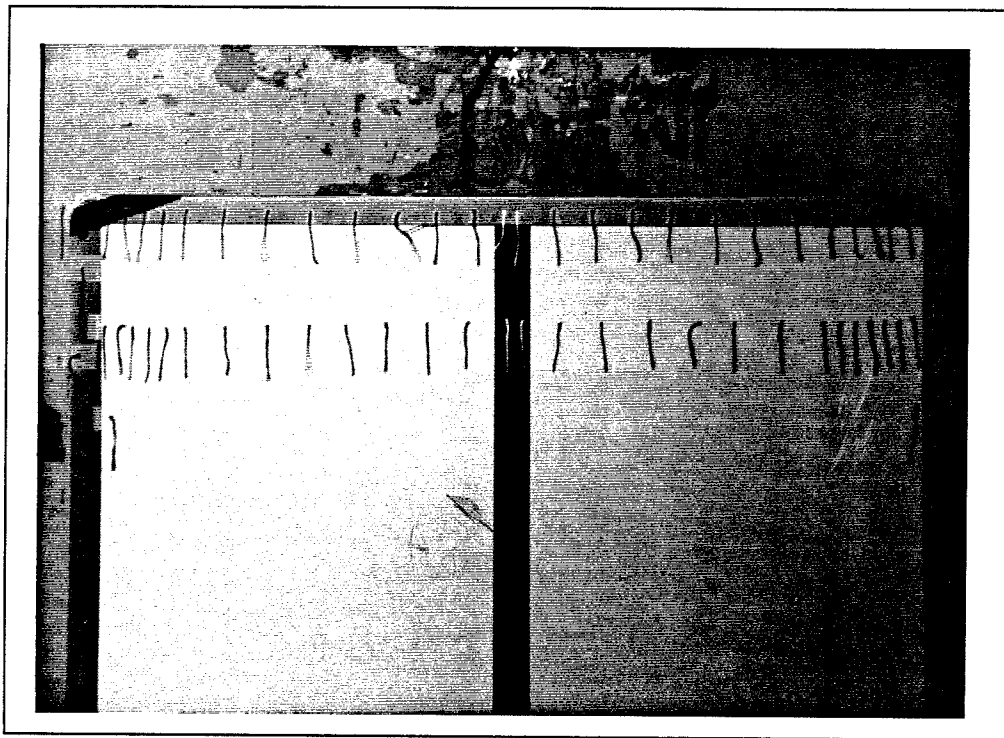
Figure 3. Fluttering of Tufts on Leading Edge of Ground Plane at 48 km/h
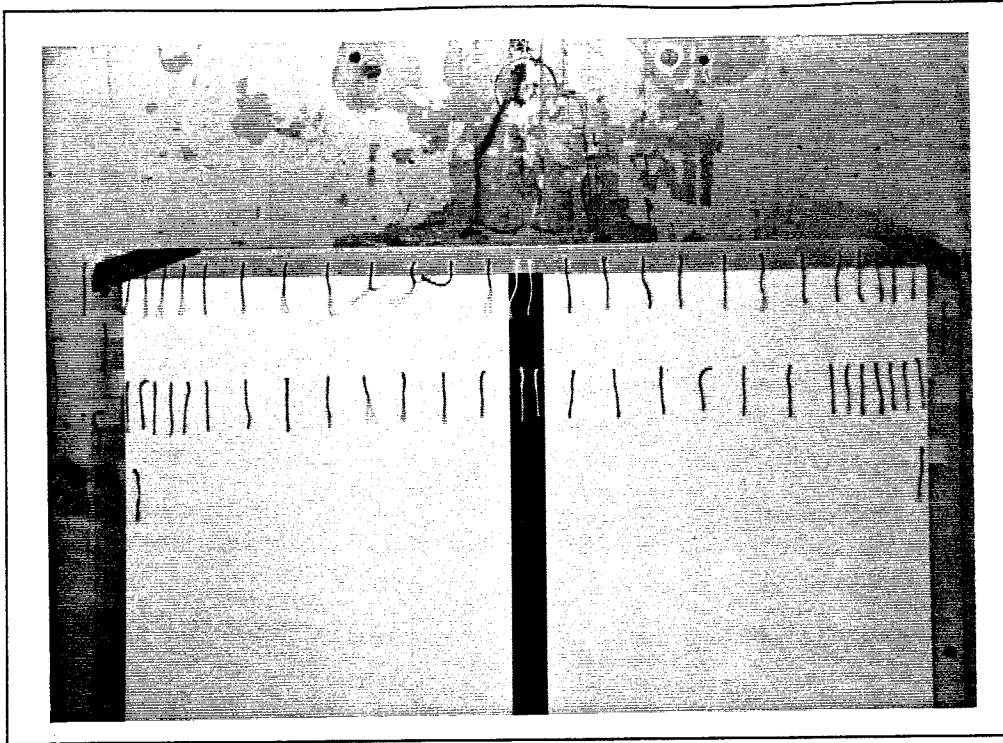
Figure 4. Flow Reversal and Fluttering of Tufts Along Leading Edge of Ground Plane at 56 km/h

4. Pressure data

Another method used to observe the quality of the flow in the tunnel was through the use of

pressure measurements. At several cross sections along the tunnel, static pressure ports were

instrumented and connected to the pressure measurement system. The locations of the tunnel

stations and pressure ports are shown in Figure 5. Most of the ports at a station were at nearly the

same angular position as ports at other stations. These ports located at the same angular position,

together formed a "streamline" (in a non-formal sense) along the tunnel wall. The ports comprising

the "streamline" are also shown in Figure 5. The ground plane was installed for the collection of

the pressure data. Data was acquired at 32, 48, and 64 km/h. The pressures recorded were
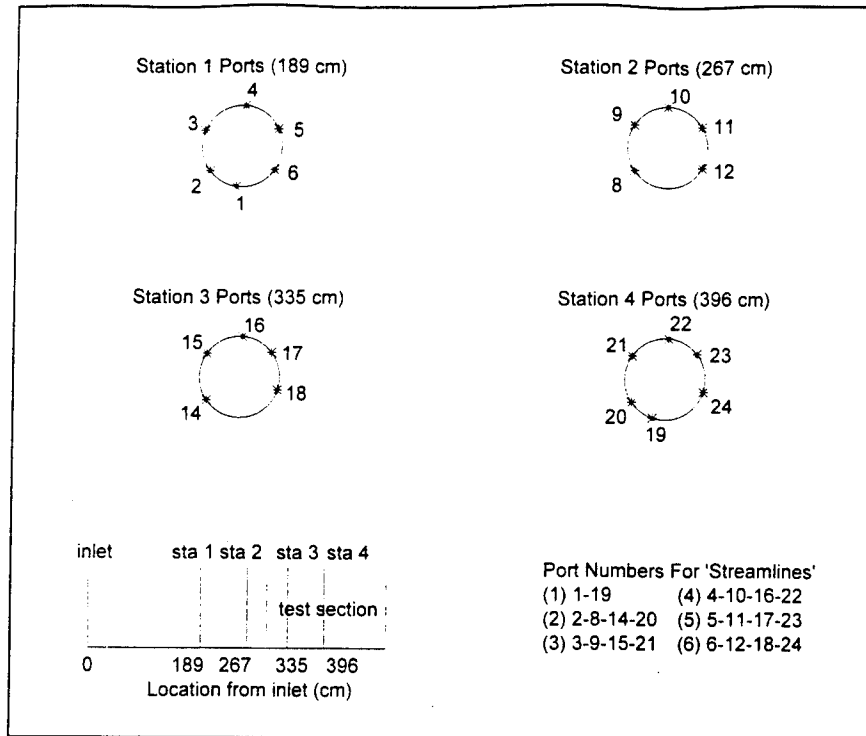
Figure 5. Static Pressure Port Locations

pressure differences from the atmospheric pressure. The consistent pressures along each "streamline" indicated the relative steadiness of the flow as shown in Figures 6-11. Anomalies in the flow around stations 16 and 20, 24 were attributed to irregularities in the tunnel walls from openings such as windows, doors, open holes, and rough surfaces.

5. Dynamic Pressure Behavior

Since tunnel speeds for the bicycle tests varied less than 32 km/h, good quality dynamic pressure data was required. Therefore, a quantitative study of the dynamic pressure was accomplished.

The objective of this test was to determine the behavior of the dynamic pressure at low speeds. Several combinations of tunnel configurations were tested in order to determine the best
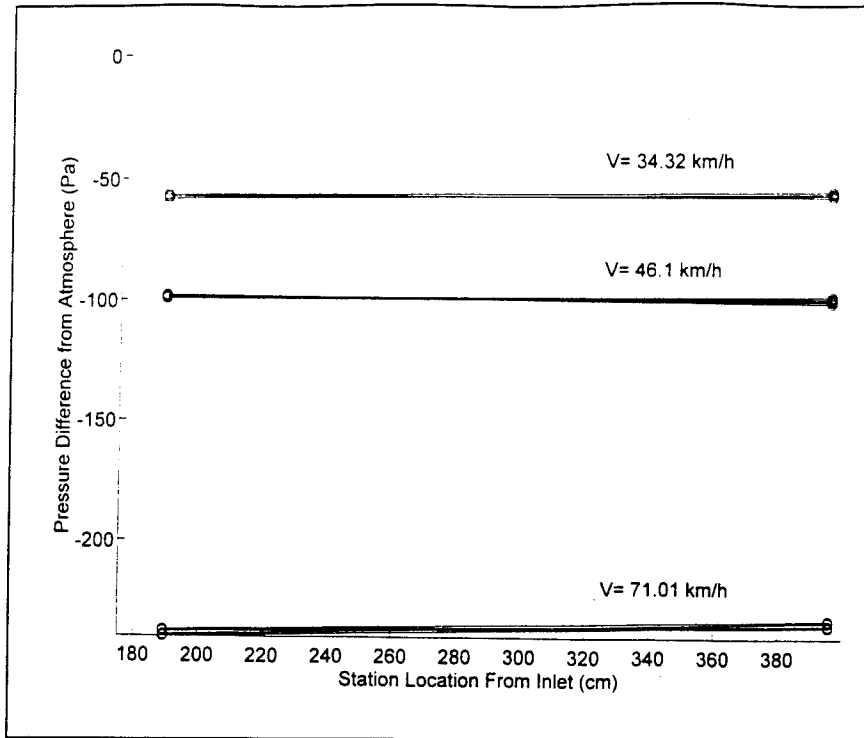
Figure 6. Differential Pressures Recorded Along "Streamline" 1 (5 Data Points)
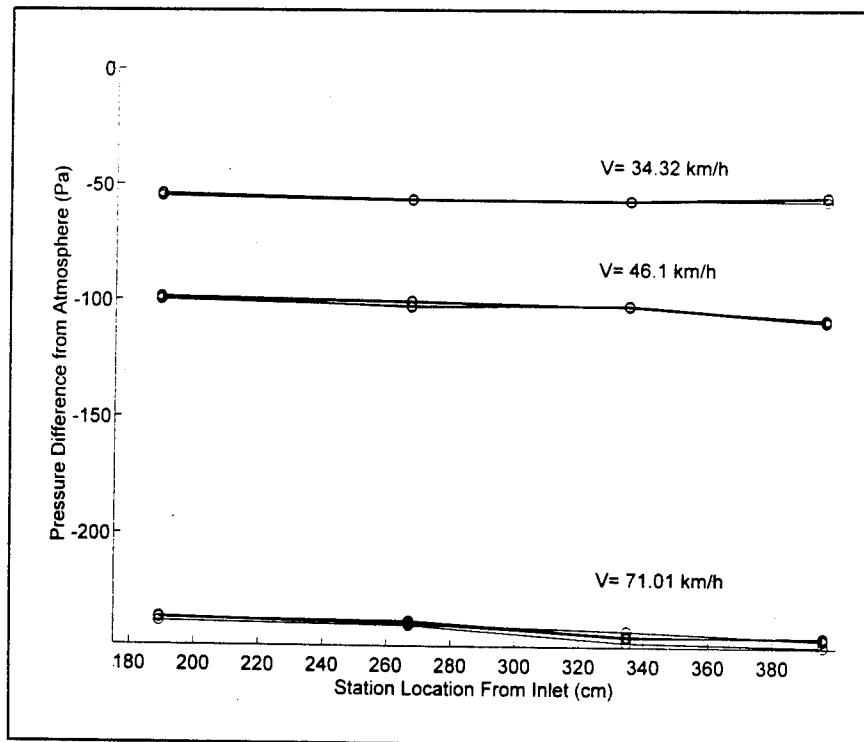
Figure 7. Differential Pressures Recorded Along "Streamline" 2 (5 Data Points)
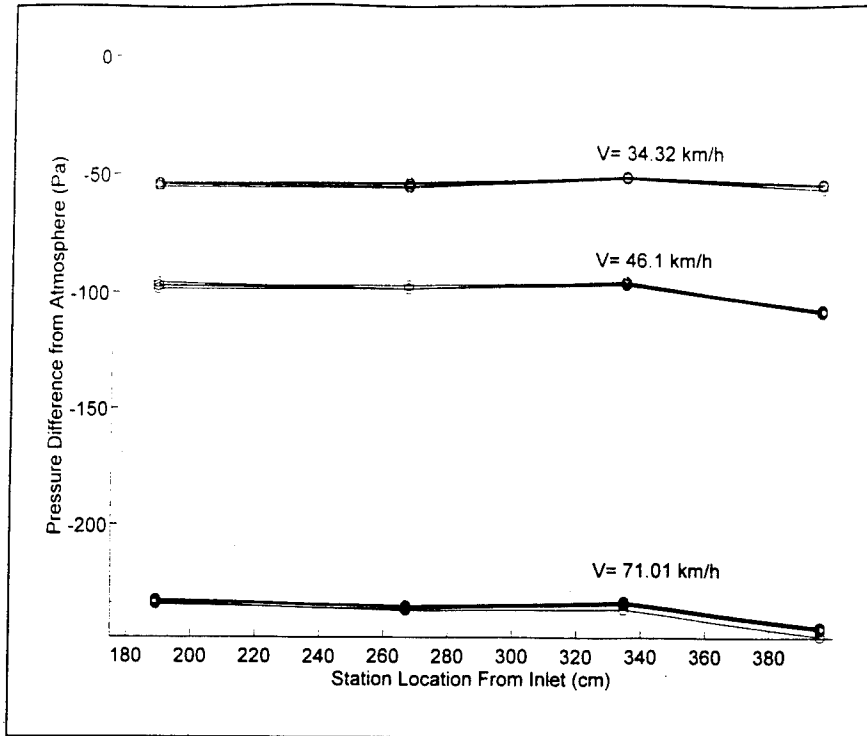
Figure 8. Differential Pressures Recorded Along "Streamline" 3 (5 Data Points)
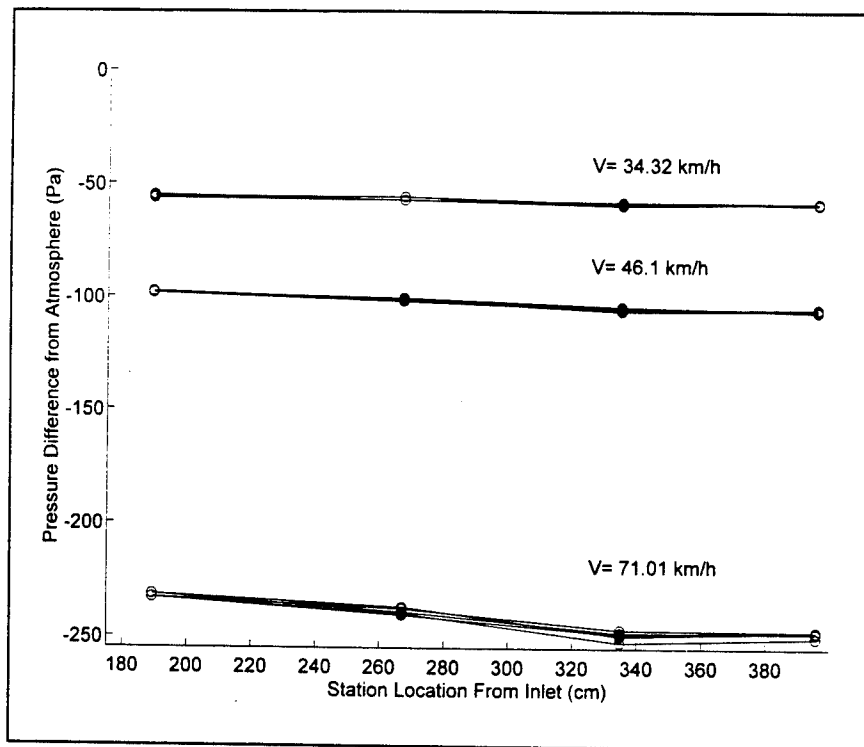
Figure 9. Differential Pressures Recorded Along "Streamline" 4 (5 Data Points)
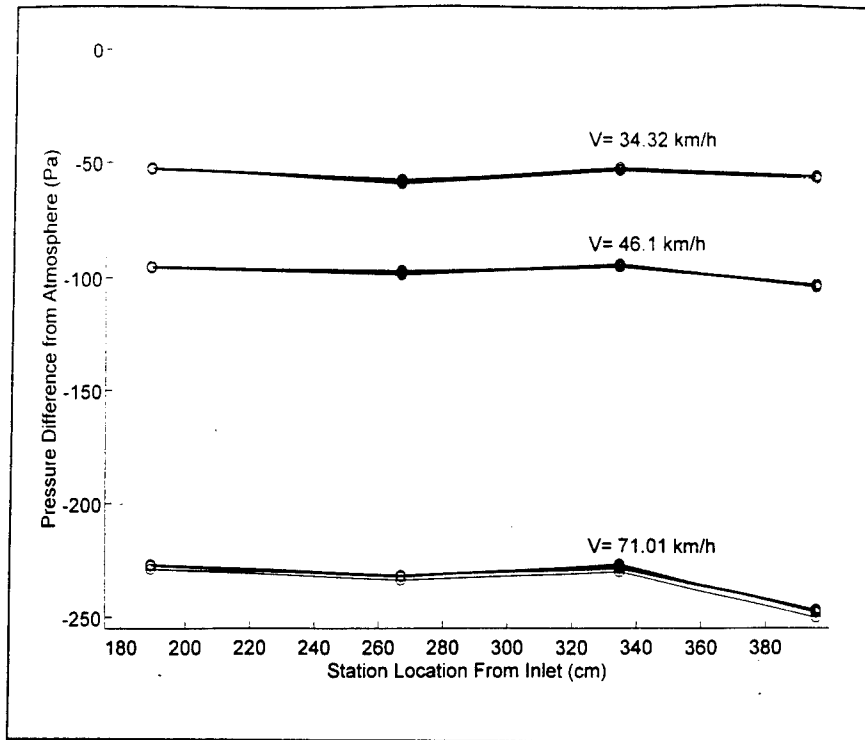
Figure 10. Differential Pressures Recorded Along "Streamline" 5 (5 Data Points)
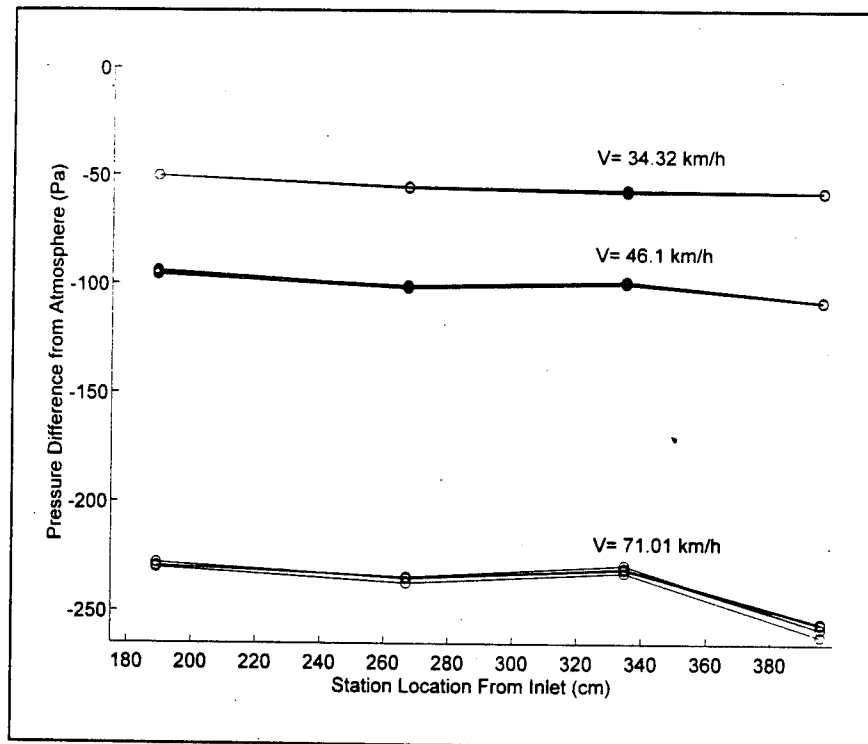
Figure 11. Differential Pressures Recorded Along "Streamline" 6 (5 Data Points)

16

configuration for low-speed experimentation. Variables consisted of front and rear motors and the position of the flow-straightening vanes at the tunnel inlet.

5.1. Motor Set

Both the rear and front motor sets were run in order to assess the difference between the resulting dynamic pressures. A sample time history of the resulting data is shown in Figure 12. The dynamic pressure, q, was corrected for pressure, temperature, and solid and wake blockages. In addition, for each run, the dynamic pressure was divided by its average value to normalize the data. This normalization allowed each run to be directly compared. The plots clearly indicated that the rear motor set produced the smoothest flow in the tunnel. The oscillations present in the plots for the front motors were probably due to the close proximity of the fan blades to the test section and dynamic pressure transducers and the fact that two opposing fan blades were missing.
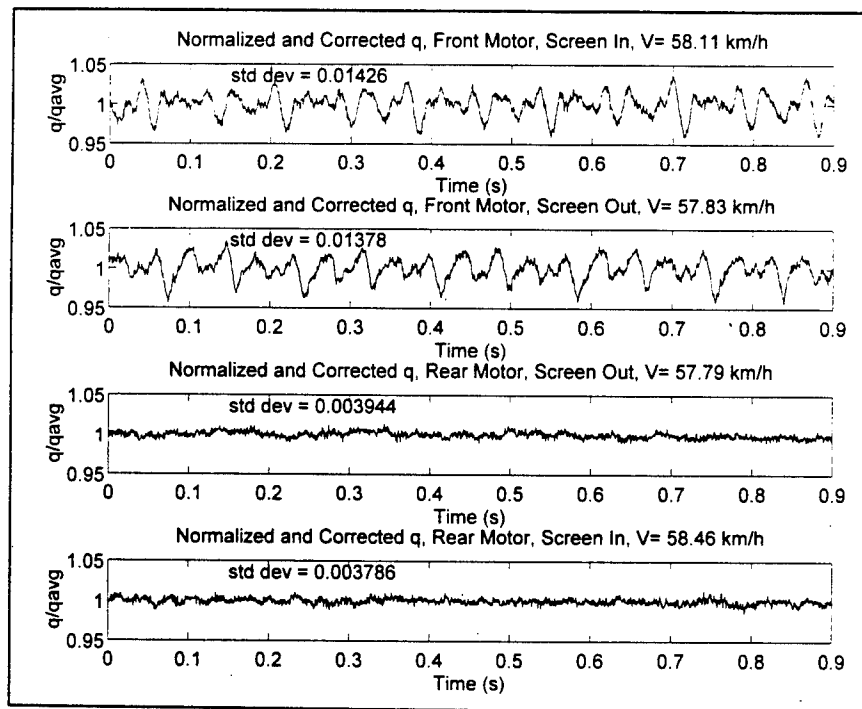
Figure 12. Time Histories of Tunnel Dynamic Pressure for Various Tunnel Configurations

5.2. Screen Position

Additional tests were run with the straightener positioned at the inlet (the "in" configuration) and 3.0 m from the inlet ("out") using each set of motors. A sample of the time histories is shown in Figure 12. Although no difference was seen in the dynamic pressure time histories, there were clear indications of turbulence in the test section during the "out" configuration tests. These tests were completed with the bicycle mounted in the tunnel. The bicycle, mounted off of a large moment arm, magnified any turbulence effects in the tunnel air flow. With the screen in the "out" position, the bicycle was clearly less stable. The bicycle experienced larger oscillations that were generally less damped with the screen "out." On occasion, the oscillations were divergent. With the screen "in," the oscillations were well damped and never divergent.

5.3. Conclusion

Using the results of the tufting test, wall pressure port test, motor set test, and straightener position test, the tunnel was considered adequate for low speed bicycle research. The best configuration for conducting the tests was using the rear set of motors and running with the straightener "in," located next to the inlet of the tunnel. As long as good sampling techniques were used, oscillations in dynamic pressure averaged out over the course of the point data collected.

Chapter 3. Phase II - Vertical Sting and Data Acquisition System

Several problems, including lack of balance sensitivity, large cantilevered load, and limited insight into the time history of the data, prevented the use of the existing wind tunnel data collection system and horizontal sting. First, the existing balances available at AFIT were not sensitive enough to measure accurately the drag and the small changes in drag expected from this experiment. In addition, the moment the bicycle would impart to a balance on the existing horizontal sting was too large for the sensitive balance required. And finally, the existing data system only provided the average of the values collected (no time histories). A detailed look at the data was necessary to ensure the quality of collected data. These problems, coupled with the acquisition of National Instruments' data collection system called LabVIEW®, led to the decision to create an entirely new data collection system and vertical mounting system, or vertical sting, for the wind tunnel.

Since the primary force of interest was drag, a simple, but optimally designed, unidirectional flexure and vertical sting (see Section 2) were developed. The new data system (see Section 3) was versatile enough for the data collection required, adaptable to the particularly unique needs of the experiment, and provided ample insight to the acquired data.

1. Scope

The vertical sting design was limited in complexity. The design was limited to providing a means of collecting drag force data using a unidirectional flexure. The new data acquisition system was intended to provide a means of collecting and reducing the data required for this experiment. It was not intended to be universally applicable to all future experiments in the wind tunnel. The system, designed with flexibility in mind, was versatile enough to work with both a

1.27 cm (0.5 in) six-component. strain gage balance and the unidirectional flexures specially designed for this experiment.

2. Vertical Sting and Unidirectional Flexure Design

The vertical mounting system and flexure were not unlike the horizontal sting. Instead of suspending the model from behind, the vertical system supported either the bicycle or the cylinder from the top. The system consisted of a mounting plate, sting, and extender bar. The setup and flexure are described below.

2.1. *Mounting Plate, Sting, and Extender Bar*

A 1.27 cm (0.5 in) thick aluminum plate measuring approximately 76 x 81 cm (30 x 32 in) served as the mount for the sting and flexure and was attached to the top of the wind tunnel above the test section. A clamp attached to the plate held the sting in place. A sturdy 3.2 cm (1.25 in) diameter steel pipe served as the sting. A collar was placed on the sting above the clamp (see Figures 13 & 14). Both vertical and rotational (heading angle) position were independently adjustable. The end of the sting accepted a 1.27 cm (0.5 in) flexure or balance using set screws. An extender bar was attached to the other end of the balance. For the cylinder, a brass fitting machined to match the taper of the 6-component balance was attached to the extender bar. The cylinder was secured to the fitting. For the bicycle, the extender bar attached directly to the bicycle mount.

2.2. *Unidirectional Flexure*

Capt Brian Parker (Parker, 1994) designed the unidirectional flexures used in this thesis. Each flexure was specifically designed for each application to give the best sensitivity for the
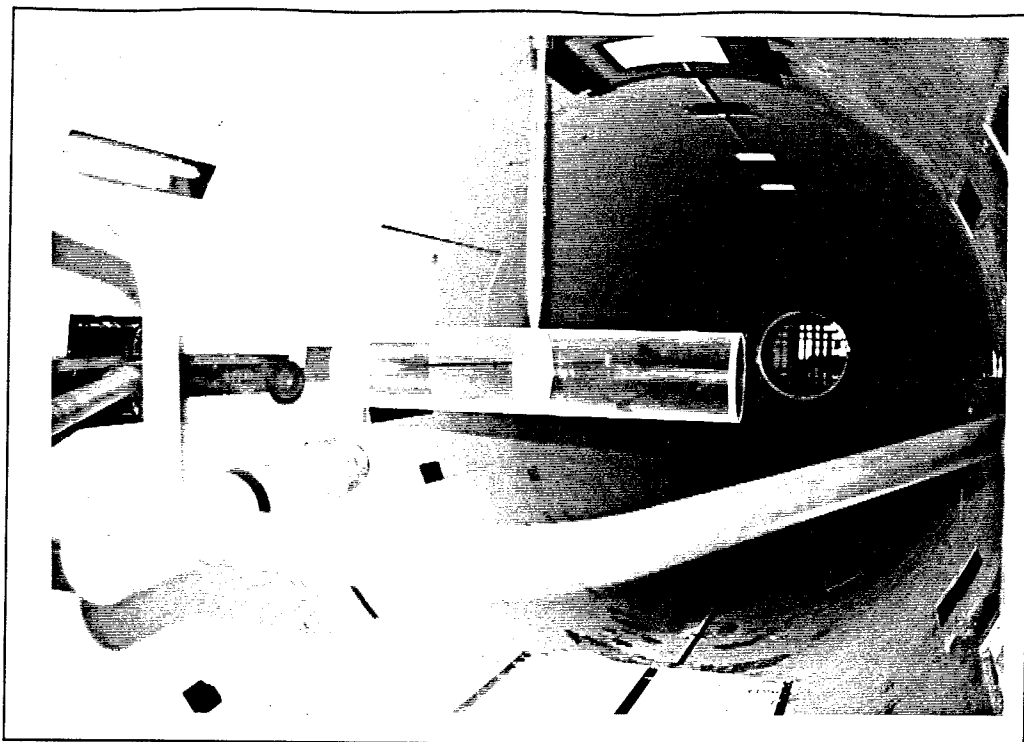
Figure 13. Cylinder Model Mounted on the Vertical Sting
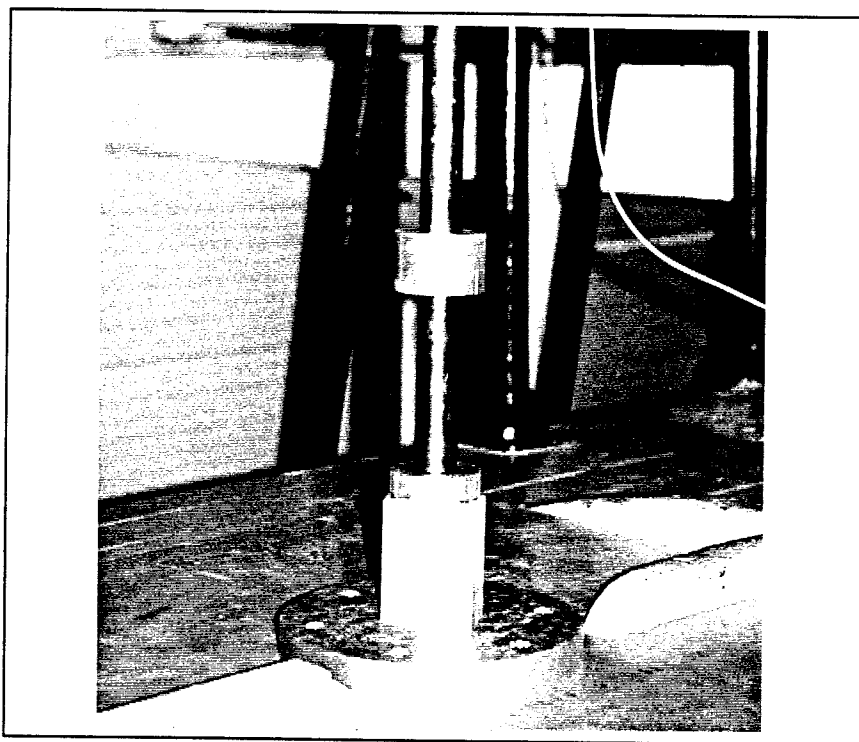
Figure 14. Vertical Mounting System Collar, Clamp, and Mounting Plate

expected drag load. In order to maintain sensitivity and prevent carrying large moments due to heavy models on the horizontal sting, the flexures were designed for installation on the vertical sting.

The design was essentially a vertically-mounted, cantilevered beam with an axial load. The model weight provided the axial load while the tunnel air supplied the normal load. Although maximum sensitivity was the design goal for the flexure, the flexure still had to support the axial load and moment of the model in a dynamic environment.

The flexures were fabricated from aluminum and instrumented with a full bridge balance using MicroMeasurement N2A-13-T006N-350 strain gages. These 350 Ω gages (2.08 nominal gage factor) were of open face construction and were both creep and self-temperature compensated. The flexures were designed to provide greater accuracy than that of the data acquisition system. Therefore, the flexures did not reduce the overall accuracy of the system.

3. Data Acquisition System

3.1. *Equipment*

The LabVIEW® data acquisition system consisting of a data acquisition board and application software. When used together, the system provided a complete, and versatile, data acquisition and reduction system.

3.1.1. AT-MIO-16(L) Data Acquisition Card

The AT-MIO-16(L) data acquisition card was the heart of the data acquisition system. This card was capable of making low-level voltage measurements. The card had a 12 bit A/D

converter and 16 analog inputs with data acquisition rates of up to 100 kHz. This highly accurate data card rejected noises as low as 0.1 LSBrms with a typical DNL of 0.5 LSB.

In differential mode (only 8 channels available), each channel referenced its own ground signal. Differential mode was recommended for use when the input signals were less than 1 VDC, input leads were greater than 4.6 m (15 ft), inputs required a separate ground reference, or in the midst of an electrically noisy environment.

The programmability of the card was a convenient feature. Each channel could be individually programmed to a particular gain as listed in the user's manual and reproduced in Table 4. This allowed the user to specify the voltage range of the sampled data in order to maximize the precision of each channel.

Table 4. AT-MIO-16(L) Data Acquisition Settings

Gain	Range	Precision	Acquisition Rate
1	±10.0 V	4.88 mV	100 kHz
10	±1.0 V	488 µV	100 kHz
100	±0.1 V	48.8 µV	70 kHz
500	±20.0 mV	9.76 µV	20 kHz

3.1.2. LabVIEW® Software

The LabVIEW® software is a program development application that uses a graphical programming language, G, to create programs in block diagram form. This software package, when used with the AT-MIO-16 data acquisition board, provided the capability to acquire completely, reduce, and output data. The software, designed to run in the Windows® environment, uses the icon concept.

Building an application package was composed of two parts. The first part was called the front panel. The other part was the wiring diagram. The front panel contained all of the switches, controls, indicators, and graphical outputs the user needed to control the operation of the package. The wiring diagram was just as the name implies: the signals on the lines were directed along the wiring path to icons, or objects, that applied a function to the signal.

Once a package was built, it could be reduced to an icon itself for inclusion into another application. This allowed the user to build layered applications. The software package itself managed the compiling and debugging, if required, of the user written application.

3.2. Requirements

Several requirements were drawn up for the design of the system. First, and foremost, it had to be flexible enough to handle both the commercial, six-component balance and the specially-designed, single-component balances used in this experiment. In addition, the system had to be capable of detecting the small voltages expected from the output of the strain gage flexure. And finally, the system needed to provide insight into the collected data much like a time history record would provide. The LabVIEW® software not only met these conditions, but also far exceeded the needs and expectations of providing a straightforward means for handling the acquired data.

3.3. LabVIEW® System Application

The existing wind tunnel data system served as a model for the new system. The new data acquisition system was broken down into three separate parts. The first part was for balance calibration. The next part was for data collection. And the final part was for data reduction. The newly developed system met all of the design requirements.

In addition. the new software used a more accurate and versatile means of data handling that was available in the existing data acquisition package. Whenever possible. the strain gage voltage data was normalized by the gain of the channel. input excitation. or dynamic pressure. Normalization was accomplished by dividing the strain gage voltage data by the average of the indicated quantity (e.g. normalization by the input excitation means that the strain gage voltage data was divided by the average input excitation used to acquire the data). This ensured that changes experienced in the data acquisition process (e.g. small changes or drift in the input excitation due to an unregulated power supply) would not affect the results. This normalization process ensured that the data was as accurate as possible, a definite advantage for observing small changes in drag. In addition, it ensured that data collected with different parameters (e.g. slightly different input voltages) could be accurately reduced, compared, or used with other data.

3.3.1. Calibration

Calibration of the gages was typically accomplished first. Each balance direction was calibrated to obtain the linear relationship between the applied force and output voltages of the gage. Both primary and secondary, or cross correlations, were obtained for multiple gage balances. The resulting slopes were then used during the data reduction to determine the force of the applied aerodynamic loads. Tare data could also be taken for use in the reduction routines. The data was normalized for gain and input excitation.

3.3.2. Data Collection

Data was collected in a time-correlated fashion, unlike the old data collection system where each channel's data was wholly collected before the next channel's. A zero point was taken to account for any offsets while providing each run a reference starting point. As the data was

collected. the time history of each data channel was displayed so that the data could be qualitatively examined for anomalies. All the data was averaged for use in the reduction routines. Filters and other data massaging techniques could also be applied to the data at this stage. All of the time history data was saved for later use or analysis.

3.3.3. Data Reduction

Once all the data was collected, it was reduced using various user-selected, tunnel correction factors as described by Rae and Pope (1984). The data was normalized at this point for input excitation and dynamic pressure. The reduced data was output to an ASCII file either with or without tabular headers. Although no quality graphics program was available with the LabVIEW® software, the data was graphed using Matlab®. Several Matlab® data reduction and graphing programs were developed for use with the new data collection system.

3.4. Verification

Verification of the proper operation of this new data system was accomplished through a rigorous set of data manipulation tests. All parts of the data reduction routines, from calibration to final corrected C_d values, were verified using the new system. Identical results were obtained from both the old data acquisition system and the new LabVIEW® system routines. Even critical intermediate results in the LabVIEW® routines were verified as accurate.

26

Chapter 4. Phase III - Cylinder Data Verification

This phase details the verification of the unidirectional flexure and vertical mounting system using a cylinder. Section 1 covers the scope of the phase while section 2 covers the new equipment used in this phase. Section 3, Experimental Procedures, includes calibration, data acquisition, and data reduction. And finally, Section 4 finished the phase with results from the cylinder tests.

1. Scope

Since the cylinder has some well-documented drag characteristics (Hoerner, 1965), a comparison between the data collected and these documented results was used to verify the proper operation of the unidirectional flexure and vertical mounting system. The data acquired with the unidirectional flexure was also compared with data collected with the 6-component balance and the horizontal sting.

2. Equipment

The ground plane (see Chapter 2, Section 2.3) was installed for all work with the cylinder. All data was collected using the new data system that was verified in the previous phase. Additional key equipment used for these tests is described below.

2.1. Cylinder Model

The cylinder model had an aspect ration of 4.8, was constructed of plexiglas, and measured 61 cm (24 in) long and 13 cm (5 in) in diameter. An aluminum insert in the middle of the cylinder accepted a 1.3 cm (0.5 in) flexure. The ends of the cylinder were plugged with a removable plexiglas insert. The overall weight of the cylinder was near 15.6 N (3.5 lb$_f$).

2.2. Horizontal Sting and 6-Component Balance

The horizontal sting was the typical sting used in the tunnel for other experiments. It consisted of a "u"-shaped support with the sting extending from the center of the "u" (see Figure 13 (foreground)). The 6-component balance was mounted to the end of the sting. The balance was designed to be inserted into the model where it was fastened with set screws. The sting was set to 0° AOA and 0° sideslip for all of the data runs.

The cylinder was installed on the horizontal sting with Able Corporation's 0.50 Mk V-E 6-component internal balance. The 6-component commercial balance measured loads of up to 890 N (200 lb$_f$), 445 N (100 lb$_f$), 222 N (50 lb$_f$) in the normal, side, and axial directions and detected moments of up to 4.5 N·m (40 in·lb$_f$), 23.7 N·m (210 in·lb$_f$), and 9.6 N·m (85 in·lb$_f$) in the roll, pitch, and yaw directions, respectively. The balance was accurate to ±1% of full scale in each direction.

2.3. Voltage Signal Recording

Each part of the cylinder tests was accomplished using different signal recording techniques. The horizontal system employed a bank of amplifiers for data conditioning whereas the vertical system used the differential mode of the LabVIEW® data acquisition card.

2.3.1. Amplifiers

A bank of Pacific Instruments Model 9355 Transducer Amplifiers was used in conjunction with the 6-component balance. These signal conditioning amplifiers were used to filter and boost the voltage signals received from the balance. The amplifiers supplied the excitation voltage to the balance strain gages. Excitation steps of 1 VDC (to 15 VDC maximum) were calibrated to within ±0.2% of full scale. Amplifier balancing was accomplished with a 350 Ω bridge with auto-

zeroing. Bridge balancing was accurate to within ±0.05% of the excitation voltage. The amplifiers offered an input impedance of 50M Ω and a source impedance of 1000 Ω. Variable gain setting on the amplifiers ranged from 1-10k with a ±0.1% accuracy and linearity of ±0.01%. The dynamic response of the amplifiers provided a -3 dB point at 1000 kHz for gains to 1k. Filtering was accomplished with a Bessel (24 dB/octave) low-pass filter using selectable filter frequencies.

2.3.2. Differential Mode

Data collected for the cylinder installed on the vertical system was collected using the differential mode of the AT-MIO-16(L) data acquisition card (See Chapter 3, Section 3.1.1). The gain control, filtering, and balancing provided by the amplifiers was not needed when differential mode was used.

3. Experimental Procedure

The procedures for collecting the cylinder data were similar for both the horizontal and vertical setups. After data collection parameters were set and a calibration was performed, the data was simply collected and then reduced.

3.1. Calibration

3.1.1. Horizontal System

Calibration was performed to determine the linear relationship between the strain gage output voltages and the applied force (weight). Calibration of the balance was done in compliance with the procedures set forth in the wind tunnel data acquisition guide for the old data acquisition system. Calibration was completed without the model installed. The axes of the balance were individually loaded in both the positive and negative directions with various weights and the

resulting output voltages measured for all six components. A 14 point incremental calibration was used for each loading to ensure an accurate calibration curve. The curve was determined from the best-fit line using a least-squares method. By measuring all six axis outputs due to the load on a single axis, balance interactions were determined (Rae and Pope, 1984:187). The calibration curve slopes were compiled into a calibration matrix for use in data reduction.

3.1.2. Vertical System

Static calibration of the vertically mounted flexure was accomplished with the cylinder mounted in position. This allowed the flexure to be preloaded with the model weight, thus eliminating any effects of creep. The calibration was simplified since there was only one direction: the secondary direction correlations were neglected. For the 6-component balance, the secondary direction correlations for the axial direction were on the order of 50 to 250 times smaller than the primary correlation. It was therefore important to have the cylinder well aligned to keep the secondary correlations to a minimum. Twisting and rolling of the model were accounted for by assuming that over the course of acquiring a data point, the average roll and twist were negligible. For calibration, a lightweight taut string was attached to the cylinder and draped over a pulley so that weights could be hung on it. The pulleys were tapped to keep friction and hysteresis to a minimum.

Both strain gage voltage and input excitation were acquired at a rate of 2400 Hz for 1 second (2400 samples) using the ±0.1 V range as shown in Table 4. The calibration was a 22 point calibration (11 points each for loading and unloading) with an average change in weight of 10% of the total expected force (15.7 N). The calibration curve shown in Figure 15 displays very little hysteresis. The curve was obtained from a least-squares, linear curve fit of the normalized data. Normalized data was obtained by differencing the normalized zero voltage from each
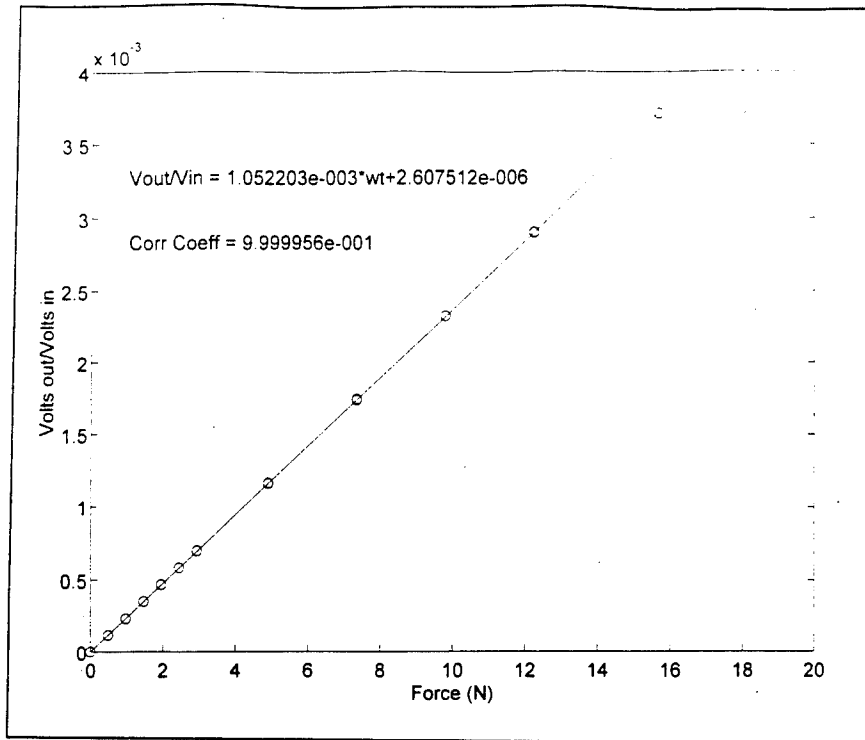
Figure 15. **Calibration Curve for the Cylinder Model on the Vertical Sting with the Unidirectional Flexure**

normalized strain gage voltage for each weight. The voltages were "normalized" by the average input excitation. The result was an output voltage per unit voltage input (a dimensionless quantity). This dimensionless quantity was plotted against the applied weight, resulting in the calibration curve shown.

3.2. Data Acquisition and Test Conditions

Testing was accomplished using the front set of motors as this phase was accomplished prior to the flow quality tests. Speeds tested included 32, 48, and 64 km/h. These particular speeds were selected as they were typical of the speeds used during the bicycle portion of the experiment. No changes to angle of attack or sideslip were made.

For the first part. the data was collected for 1 second at 2400 Hz. The 6-component balance output voltages. dynamic pressure. and input excitation (set to 6 VDC) were recorded. The amplifier settings included a gain of 100 and filtering at 3 kHz. Three data points were taken at each tunnel speed. Building barometric pressure and tunnel temperature were also manually recorded for data reduction.

For the second part, the data was collected for 1 second at 2400 Hz using the ±0.1 V input range for the data acquisition card. As before, the balance output voltage, input excitation (set to 10 VDC), and tunnel dynamic pressure were all recorded. Five data points were collected for each speed tested: idle (about 32), 40, 48, 56, and 61 km/h (20, 25, 30, 35, and 38 mph). Temperature and pressure were also measured as in the first part.

3.3. Data Reduction

The data acquired with each system was reduced in nearly the same manner using the LabVIEW® software. Data reduction typically involved a set of standard corrections for daily atmospheric pressure and temperature. The calibration curves were used to convert the acquired output voltages to engineering units. In addition to the standard corrections made, a set of tunnel corrections was usually made to account for the fact that the testing was accomplished within the confines of the wind tunnel.

3.3.1. Standard Corrections

Standard corrections were made to account for changes in tunnel temperature and atmospheric pressure. These corrections were applied to the dynamic pressure. The tunnel dynamic pressure was also corrected for solid and wake blockages.

Solid blockage is a correction for the volume the model occupied in the tunnel (Rae and Pope, 1984:353). Since the model occupied some of the area in the test section, the air flow around the model increased its velocity according to Bernoulli's equation. This increase in velocity was accounted for with the solid blockage correction, a function of model thickness, thickness distribution, and model size.

Wake blockage is a correction for the wake induced behind the model (Rae and Pope, 1984:355). The flow velocity in a wake was lower than in the freestream. According to the law of continuity, the freestream velocity increases in order to keep a constant volume of air passing through the tunnel. This higher velocity results in a lower pressure which leads to pressure gradients on the model.

The wake and solid blockage corrections made to the dynamic pressure were combined into the following equation:

$$qcorr = q \cdot \left(1 + \frac{k \cdot vol}{c^{1.5}} + \frac{axfor}{q \cdot 4 \cdot c} \right)^2 \qquad \text{(Eq. 1)}$$

where $qcorr$ is the corrected dynamic pressure, q is the uncorrected dynamic pressure, $k = 0.9$ is a body shape factor modified for tunnel test section shape, vol is the model volume, $axfor$ is the measured axial force, and c is the cross section area of the tunnel (Rae and Pope, 1984:365,367). Since the cylinder was held stationary at a constant angle of attack and sideslip, no angle of attack of sideslip corrections were made.

3.3.2. Determination of Drag

Determining the drag of the cylinder was relatively straightforward. The experimental data presented in Hoerner (1965:3-16) indicates that for the Reynolds numbers used during testing, the drag coefficient is constant. Therefore, the drag is linearly related to the dynamic pressure

$$D = q \cdot s \cdot C_d \qquad \text{(Eq. 2)}$$

where D is the drag. C_d is the drag coefficient. q is the dynamic pressure. and s is the model reference area. Therefore. best-fit lines were often obtained from a drag versus dynamic pressure plot using a first-order. least-squares. curve-fitting routine.

3.3.3. Drag Coefficient, C_d

The drag coefficient was then determined from the resulting best fit curve slope by dividing by the model reference area. Data reduction was not yet completed as additional drag corrections still needed to be made. These final correction factors were for buoyancy, induced, and support tare drag.

3.3.4. Drag Corrections

Most tunnels with closed throats have a static pressure variation along the test section due to the thickening of the boundary layer. Since the effective exit area was decreased because of this boundary layer, the exit pressure was lower. This led to a drag on the model due to the pressure difference. This effect, known as buoyancy, was removed from the drag calculation (Rae and Pope, 1984:350). The buoyancy correction factor had a value of -0.375 N (-0.084 lb$_f$) and was obtained from the following equation:

$$D_b = -\left(\frac{dp}{dl}\right) \cdot vol \qquad \text{(Eq. 3)}$$

where D_b was the buoyancy drag; $\dfrac{dp}{dl}$ was the slope of the longitudinal static pressure curve where dp was the change in static pressure and dl was the change in the jet length; and vol is the volume of the model body.

34

The flow (streamlines) caused by the vortices shed off of an object in the freestream extends to infinity. Since this flow is restricted by the tunnel wall. an induced drag correction is used to account for this phenomena (Rae and Pope. 1984:376). This correction factor was typically on the order of 2×10^{-6} and was obtained from the equation:

$$C_{di} = \frac{s}{8 \cdot c} \cdot C_l^2 \qquad \text{(Eq. 4)}$$

where C_{di} was the induced drag coefficient, s was the model reference area, c was the tunnel cross section area, and C_l was the lift coefficient in the body axis. Since the correction uses C_l, which was not available for the unidirectional flexure, this correction was made only for the 6-component balance data.

And finally, the last correction in drag was due to the drag effect of the support structure. Since the 6-component balance was mounted directly inside the model, no support structure added drag to the model. However, for the vertical sting, the cylinder was mounted off of a 30.5 cm (12 in) extender bar hanging below the unidirectional flexure. Therefore, the flexure detected the drag of the extender bar as well as the drag of the cylinder. The drag associated with this bar was from Equation 2 with a C_d of 0.83 based on a three dimensional cylinder with a length to diameter ratio of 9.6 (Hoerner, 1965:3-16).

One final note on the corrections. Although there was some interference drag effect due to the connection between the model support and the model, it was neglected in this experiment as it was assumed minimal and difficult to determine.

4. Results

The reduced cylinder data is presented for the two different mounting systems. Both data sets were compared to past experimental data. Accuracies of the data are also presented.

4.1. Overall Drag and Repeatability

Aerodynamic drag for the cylinder using the horizontal mounting system (6-component balance) is shown in Figure 16. Multiple data points at each speed are shown along with the best linear fit line through each set of data. The data was shown to be repeatable by the two different sets of data taken at two different times.
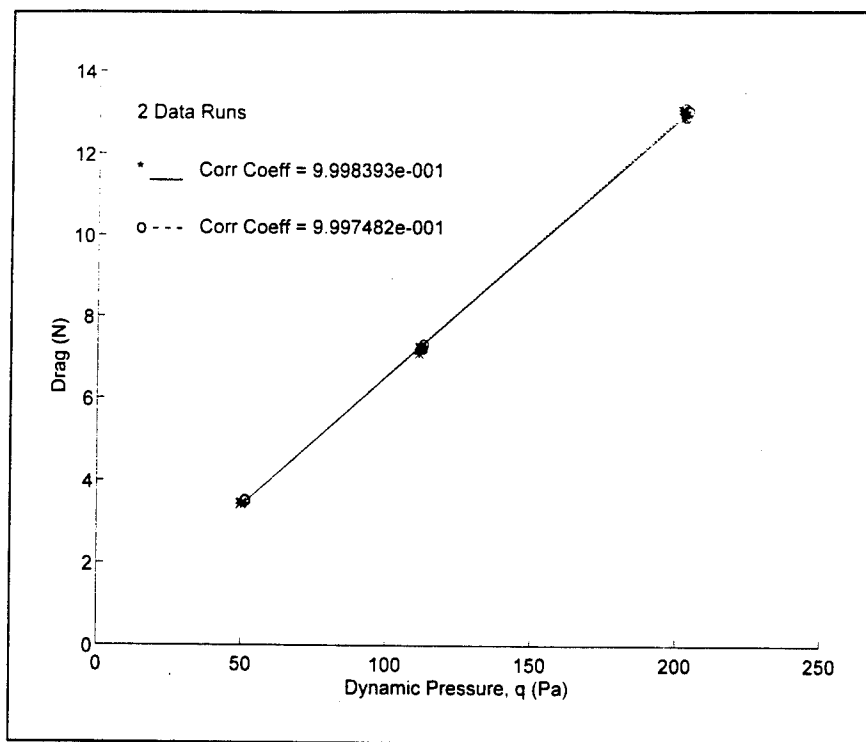
Figure 16. Drag on a Cylinder Mounted on a Horizontal Sting Using a 6-Component Balance

For the vertical mounting system, Figure 17 shows the drag results. Again, the results were clearly shown to be repeatable by the two different runs. The excellent linearity of the experimental data was apparent with the best fit lines having correlation coefficients of 0.999 for both sets of data.
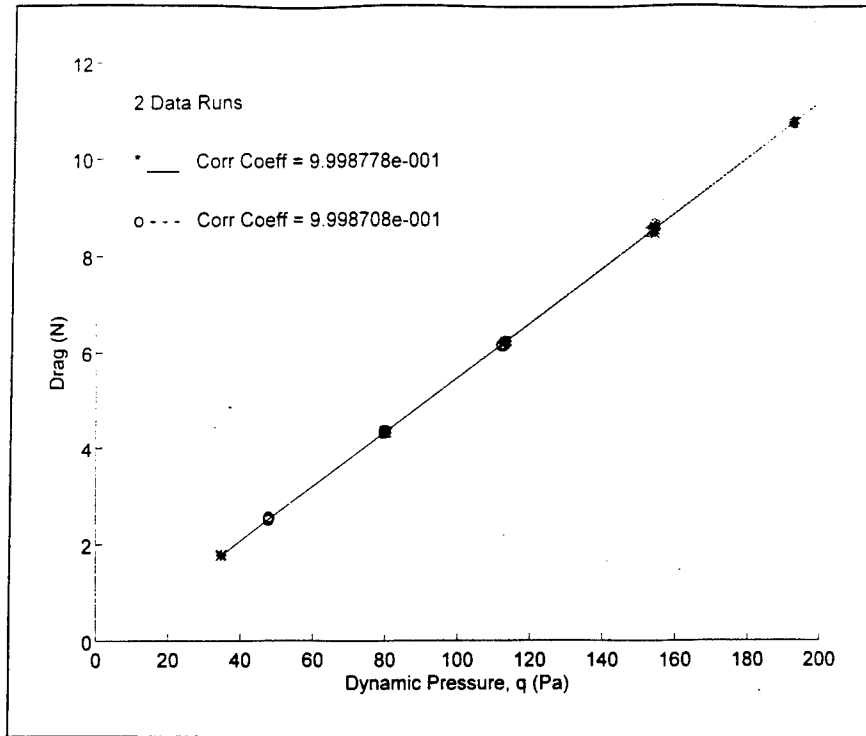
Figure 17. Drag on a Cylinder Mounted on a Vertical Sting Using a Unidirectional Flexure

4.2. Comparison with Prediction

For a three dimensional cylinder, Hoerner provided past experimental data at a Reynolds number of 1×10^5 showing the drag coefficient to be a constant 0.75 (Hoerner, 1965:3-16). Figure 18 graphically represents the results of the two systems along with the past data. Clearly, the data did not fit as well as one would have hoped. Figure 19 shows the differences between the data and the literature data. At near 40 mph, the 6-component balance system differed from the literature data by 1.3 N while the unidirectional flexure differed by only 0.55 N. Note that the difference for the optimized unidirectional flexure was nearly a third of the commercial balance. With accuracies of ±2.22 N and ±0.05 N (0.012 lb$_f$) for the horizontal and vertical systems (see Appendix A), respectively, the data gave good comparison with past data. Drag coefficients for the cylinder with
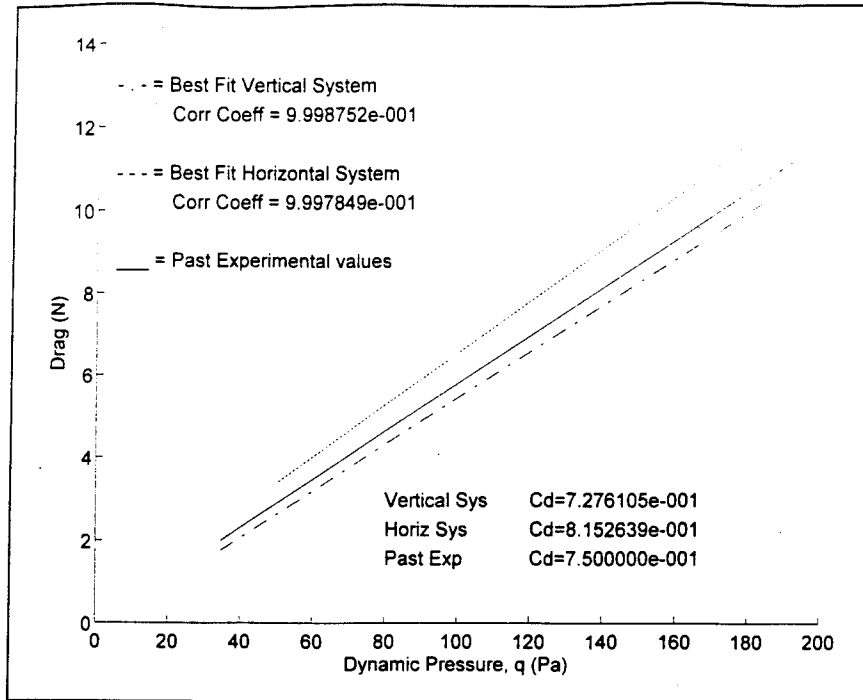
Figure 18. Comparison of Cylinder Drag Obtained Using Both a 6-Component Horizontal Balance and a Unidirectional Vertical Flexure with Past Experimental Values
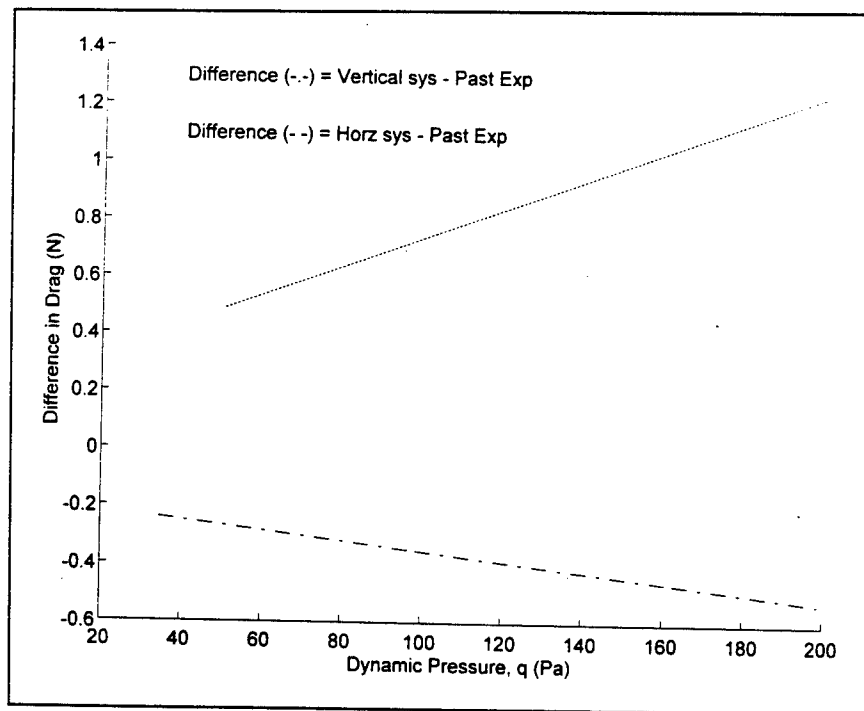
Figure 19. Graphical Representation of Difference Between Past Experimental Cylinder Drag Data and Data Collected with the Horizontal and Vertical Systems

the vertical and horizontal mounting systems were 0.73 and 0.82, respectively, as observed from Figure 18.

Although the data fell outside the error band for the unidirectional flexure, it was quite probable that the difference was due to the estimation of the corrections, especially the tare correction, and the lack of an interference correction. Recall that the tare correction for the extender bar was estimated (see Section 3.3.4) with a drag coefficient of 0.83. The calculation did not account for the fact that the ends of the bar were attached to the brass fitting and the flexure. If these objects had been included in the tare correction, the drag for the vertical system would have been higher, thus decreasing the difference between the literature values and those collected using the vertical system.

4.3. Summary

Overall, the drag of the cylinder for both systems was accurate to within the uncertainty of the gages. The unidirectional flexure gave better results than the commercial balance, as expected, because of the optimized design. For these results, the unidirectional flexure and vertical mounting system appeared to render accurate results when compared to past experimental values for a 3-dimensional cylinder. Therefore, the system was deemed satisfactory for use in the next phase; determining changes in drag on a bicycle due to varying fork spacing.

Chapter 5. Phase IV - Bicycle Fork Spacing Experiment

The groundwork was complete for bicycle testing. The tunnel was capable of producing steady, uniform flow for low-speed bicycle testing. A data acquisition system and vertical sting were in place. The data collection and reduction programs had been verified using a cylinder test model. Sections 1 and 2 review the objective and scope of the test. The experimental apparatus is summarized in Section 3. Section 4 follows with the experimental procedures including calibration, data acquisition, and data reduction. Section 5 contains a discussion of the results. And finally, Section 6 summarizes with conclusions and recommendations.

1. Objective (Problem Statement)

Recall that this phase was conducted to determine experimentally the spacing for the blades of a typical bicycle front fork that produced the minimum amount of drag. By varying the spacing of the front fork of a bicycle, the drag produced at various speeds was measured in order to define the optimal spacing for the front forks.

2. Scope

An unlimited combination of fork spacings, wheel combinations, tunnel speeds, and variable geometry fork blades could have been tested. However, this study was limited to the effect of blade spacing for one set of blades and one spinning, skirted wheel.

3. Experimental Apparatus

Only a few new pieces of equipment were required for this phase of testing. Each new piece is described below.

3.1. *Sting and Balance System*

The vertical sting was the same as described in Section 2 of Chapter 4. However, the balance was different from the one used for the cylinder in that the size of the flexure was optimized for the size of the bicycle and the drag expected on the bicycle.

3.2. *Bicycle and Mounting System*

Racing bicycles and their components come in various shapes and sizes, and there are a myriad of components available. However, in order to limit the testing, only one bicycle was tested. The bicycle system used for the test consisted of the bicycle frame and components, wheel spin apparatus, adjustable-width front fork and wheel set.

3.2.1. Bicycle Frame and Components

As indicated in Table 3, the type of bicycle ridden (standard or track) could have drastic effects on the aerodynamic drag. For testing, a track bike configuration was desired. However, since none was available, a modified road bike served as the test model. The bicycle frame used in this project was a 50 cm road bicycle previously involved in an accident which resulted in the slight bending of the down and the top tubes. It was desired that actual race conditions be matched as closely as possible to ensure accurate drag reduction trends. In order to reduce the amount of overall drag on the bicycle, making it more like that of a track bike configuration, several components were removed from the bicycle for testing. The removed components included the brakes, the brake handles and cables, seat, gear shifters, both front and rear deraillures and cables, pedals, and chain. Although removal of some of these components might seem unconventional in terms of practicality, the overall drag and turbulence level of the bicycle was reduced by their elimination. This reduced turbulence contributed to a better quality of collected data (smoother).

41

The configuration of the bicycle was unaltered between runs, except blade spacing and as otherwise noted.

3.2.2. Wheel Spin Apparatus

In order to simulate the flow of air over the bicycle as accurately as possible, spinning wheels were required. The spinning induced a velocity into the air (most notably near the wheel rim and tire) due to the boundary layer. The best possible way to accomplish wheel spin was through a moving ground plane. Since only a stationary ground plane was available, the realism was somewhat diminished. On a bicycle rolling along the ground, the point of contact with the ground has no forward velocity. The point at the top of the wheel has a forward velocity equal to twice that of the bicycle. And, a point level with the axle of the wheel is moving up or down at the same speed as the bicycle is moving forward. For a bicycle moving at 48 km/h (30 mph), this point revolves at a rate of 420.17 revolutions per minute (rpm) for a 61 cm (24 in) wheel.

The device chosen to spin the wheels was a Teledyne-Hanau air-powered dental drill rated at approximately 30,000 rpm (see Figure 20). The smooth-running drill was powered by shop air (689 kPa (100 psi) maximum) through a 0.64 cm (¼ in) pressure line and regulated with a manually-controlled flow regulator. The drive wheel was a 2.5 cm (1 in) diameter disk covered with a rubber "o"-ring. The drive unit was mounted to the bicycle down tube using a balsa wood cradle support secured with string and a tensioner system to keep the drive unit securely against the wheel to prevent slippage. The drive unit was kept as far away from the fork as possible to eliminate interaction and drag influences as much as possible.

The rate of wheel spin matched the tunnel air velocity. For example, if the tunnel speed was 48 km/h (30 mph), the wheel speed was set to 420.17 rpm, as shown above. Although no precise control over the actual rpm maintained by the drive unit was available (no electronic

42
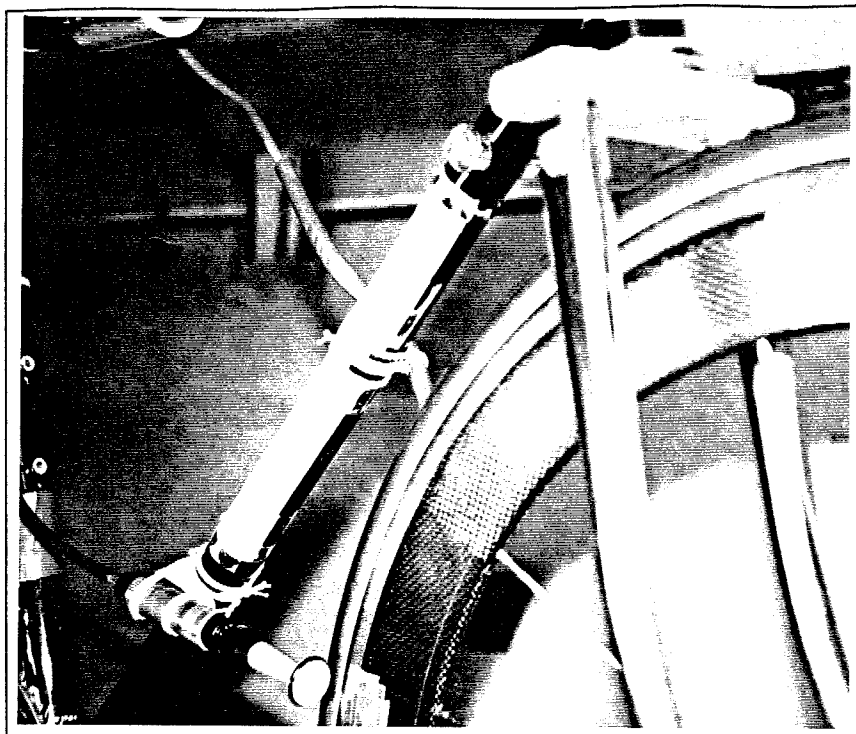
Figure 20. Wheel Spin Apparatus and Optical RPM Sensor

feedback controller), the operator was able to maintain the average frequency to two decimal

places (0.6 rpm or 0.06 km/h (0.04 mph)). The wheel spin rate was monitored by an optical sensor

mounted on the bicycle. The sensor was connected to a counter circuit and a Racal-Dana model

1992-02M Universal Timer/Counter. The sensor detected a piece of white tape on the outside of

the wheel and counted the frequency of rotation.

3.2.3. Front Fork

The bicycle was fitted with a specially designed front fork. The adjustable-width front

fork was custom made from an old bicycle front fork. All forks consist of a steerer tube, crown,

and fork blades (see Figure 1). The adjustable fork was fashioned around a new crown made out

of aluminum. The blades were cut off of the old fork, as was the steerer tube, and used on the new,

adjustable fork. The steerer tube was bolted to the center of the new crown. The blades were fitted with a bolt that was secured through a slot in the bottom of the crown. Adjustments were made to the spacing by moving the blades along the slot and resecuring them to the crown.

The blades had elliptical cross sections at the top and were tapered and reshaped to circular cross sections at the bottom near where the axle was mounted. Alignment marks at the leading edge of the blade (at the end of the major axis of the ellipse) were also added. Every 0.159 cm (0.0625 in) was marked along the front edge of the crown for alignment of the blades. Due to a design limitation of the crown, the minimum blade spacing obtainable was 2.38 cm (0.9375 in) from the centerline of the wheel to the center of each blade (overall spacing was 4.76 cm (1.875 in) from blade center to blade center). Figure 21 shows the details of the spacing geometry. Since the axle width was fixed, the fork blade angle varied between 4.7° at the narrowest spacing to 0° at the widest spacing tested.
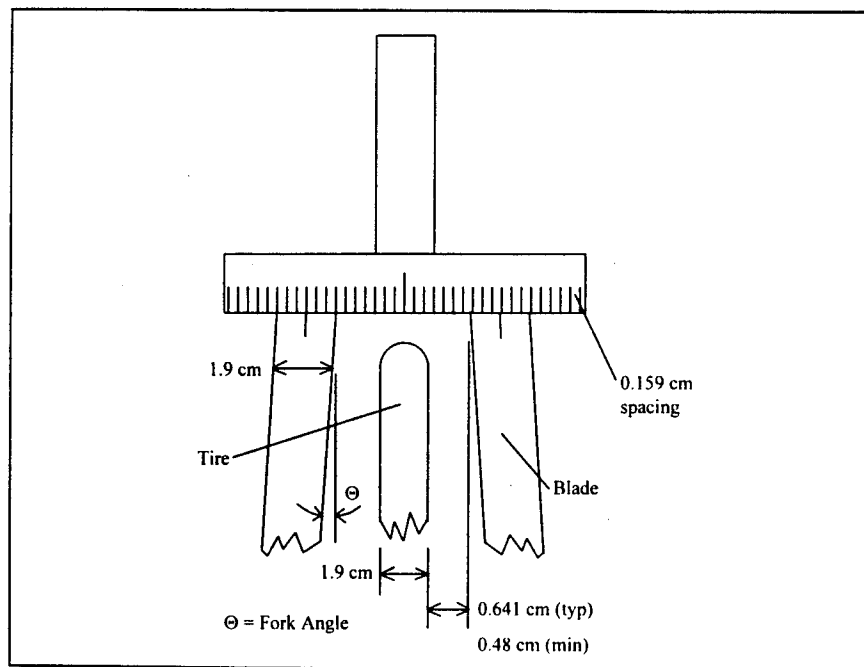
Figure 21. Adjustable-Width Front Fork Geometric Configuration

Voids in the crown were covered with tape for each run and the leading and trailing edges were covered with a balsa wood fairing to reduce the drag of the non-aerodynamically shaped crown.

3.2.4. Wheels

Two aerodynamic 61 cm (24 in) diameter wheels were supplied by the USCF. One of the wheels, a disk wheel, was composed of a composite rim and honeycomb core and carbon fiber covering (see Figure 22). The other wheel, an aerodynamic skirted wheel, consisted of a carbon fiber rim and body whose "v" shape was attached to the hub by 18 aerodynamically bladed spokes (see Figure 23).
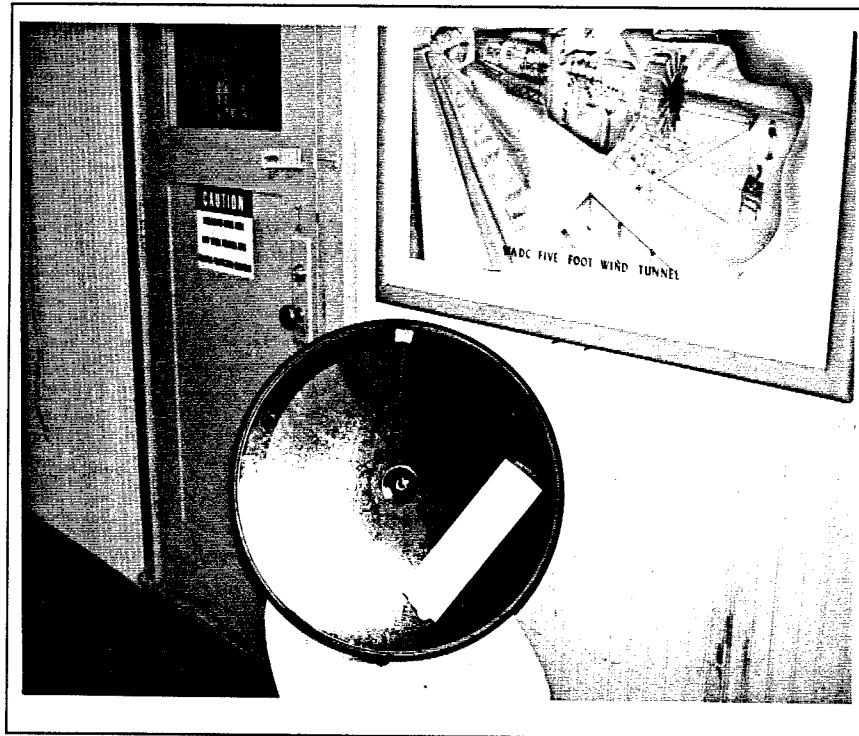
Figure 22. Rear Disk Wheel
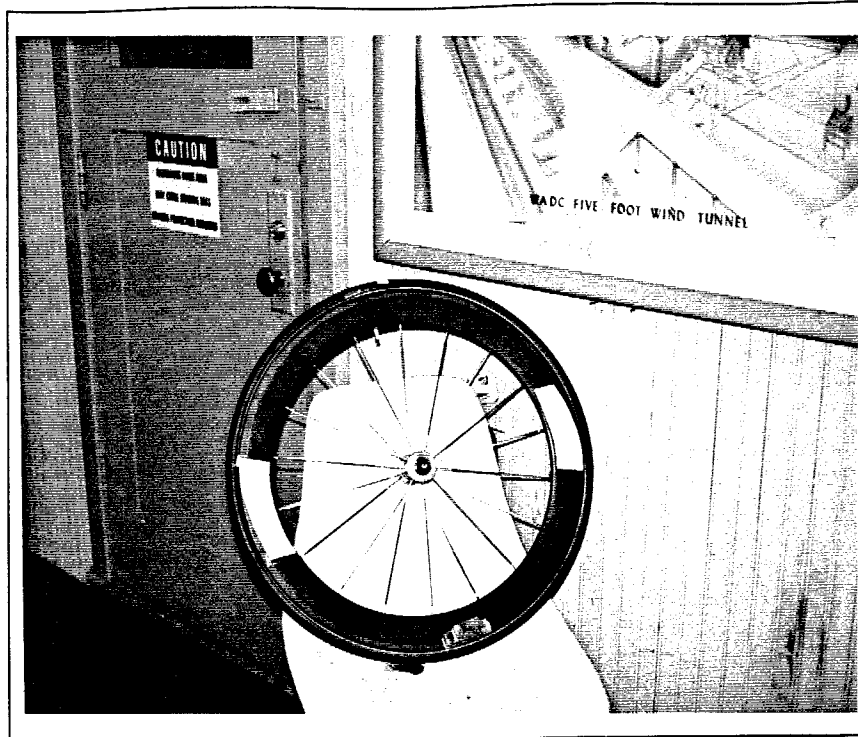
Figure 23. Front Skirted Wheel

Only the skirted wheel was tested in the front. The disk wheel was used only in the rear. Although the disk wheel could have been tested in the front position, it is unusual to see a front disk wheel due to the large side loads and instability produced by the disk wheel in the front position. The large surface area tends to develop a lift forward of the center of pressure usually resulting in difficult handling and a tendency to weathervane to the other direction, especially in a strong to moderate crosswind.

4. Experimental Procedures

The experimental procedures used for this phase were nearly identical to those used for the cylinder testing. Although most of the experimental procedures were conducted the same for the bicycle as for the cylinder, they are repeated here in order to provide the subtle differences.

4.1. Calibration

Static calibration of the flexure was accomplished with the bicycle mounted in position. For calibration, a lightweight taut string was attached to the bicycle approximately 51 cm (20 in) from the ground and draped over a pulley so that weights could be hung on it.

Both strain gage voltage and input excitation were acquired at a rate of 140 Hz for 30 seconds (4200 samples) using the ±0.1V range as shown in Table 4. The calibration was a 23 point calibration with each increase in weight not exceeding 15.6% of the total expected force (15.7 N). The calibration curve is shown in Figure 24. The voltages were normalized as they were for
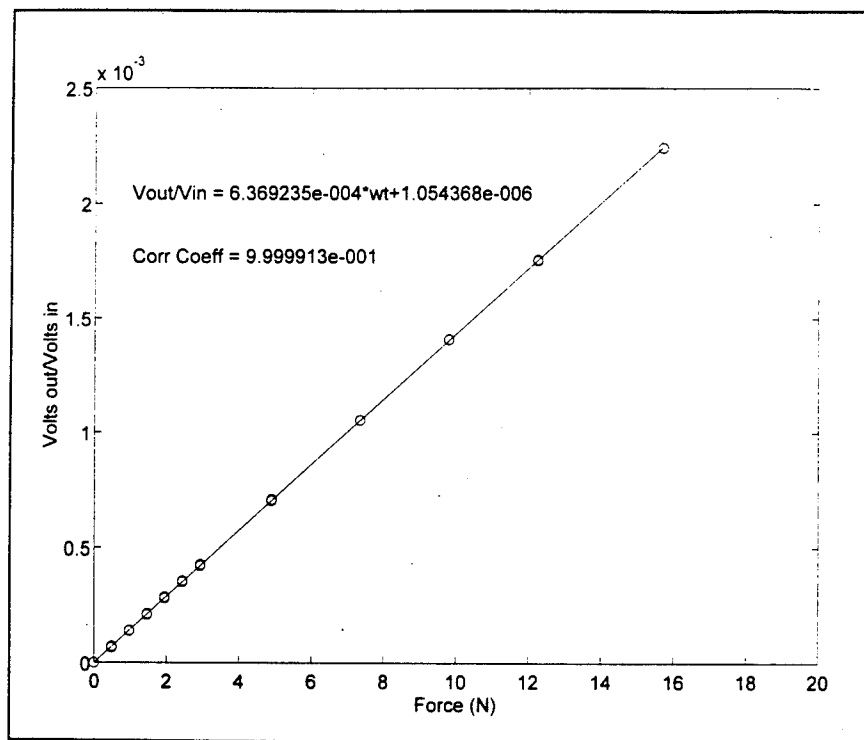

Figure 24. Calibration Curve for the Bicycle on the Vertical Sting with the Unidirectional Flexure

the cylinder (See Section 6 of Chapter 3). Static check loads of 0.49. 0.51. and 0.52 N (50. 52. and 53 grams) were used to verify that differences on the order of 0.02 N (0.0044 lb$_f$) could be detected.

4.2. Data Acquisition, Test Conditions, and Run Cases

Testing was accomplished for various blade spacings as shown in Table 5. Data was taken at tunnel speeds of 40, 48, and 56 km/h with no changes in headwind direction (sideslip). Front wheel speeds were matched to tunnel speeds at 5.83, 7.00, and 8.17 Hz, respectively.

Since frequency content of the data was not of paramount importance, the sampling frequency was chosen to be high enough to capture enough of the dynamics of the bicycle and so that the known 60 Hz building noise would average out of the data. Since the bicycle experienced random periods of lateral oscillations (approximately ±1 cm) and "calm", thirty seconds of data allowed those variations to be captured and averaged out.

4200 data samples were collected at 140 Hz. Each data channel input range was set on the data acquisition card to maximize the precision of measurements. In addition to collecting the strain gage output (±0.1 VDC), input excitation (±10 VDC), and tunnel dynamic pressure (±0.1 VDC), data collection also included tunnel temperature (±0.1 VDC) and wheel spin frequency (±10 VDC). Barometric pressure was still recorded manually. Input excitation was set just below the threshold of the data acquisition card limit of 10 VDC. A minimum of two data points per speed and configuration were collected. Wind-off "zeros" were taken for each configuration. These zero points provided a reference baseline for the run.

In addition to the fork spacing data, data was also collected to measure the effects of various factors in the setup. These factors included the effect of the spinning wheel; the effect of the wheel spin apparatus in terms of pressure in the air tubing, mass flow out of the drive unit, and

the inertia of the drive wheel: and the effect of bridging the balance and the drag on the optical

sensor and drive unit.

Table 5. Fork Blade Spacings

Spacing in cm and (in)
2.38 (0.9375)
2.54 (1.0)
2.86 (1.125) (typical)
3.02 (1.1875)
3.65 (1.4375)
4.13 (1.625)
4.60 (1.8125)
5.08 (2.0)

4.3. Data Reduction

4.3.1. Drag Coefficient

Data reduction for the bicycle was slightly different from aircraft data reduction. A drag

coefficient for an aircraft can be obtained from Equation 2. To use this same equation for a

bicycle, the model reference area would have to be determined. In order to avoid this awkward

determination, many bicycle experimentalists use a $C_d \cdot s$ value, the value of the drag coefficient,

C_d, times the reference area of the model, s. This way, the reference area of the model is not

required.

Calibration of the flexure simulates an applied load acting through the center of pressure

of a model. The actual center of pressure was unknown for the bicycle and its determination was

not possible without further investigation judged to be outside the scope of this thesis. Therefore,

the calibration was accomplished at an arbitrary location (51 cm above the ground plane) estimated

to be the "middle" of the bicycle and hence. its center of pressure. It was also further assumed that this arbitrary center of pressure did not vary with changes in the fork spacing.

Because the aerodynamic center was only estimated, the true moment arm of the applied drag force was unknown. Since this actual moment arm may have differed from the calibration moment arm. the true drag of the bicycle was unknown. Redesigning the system with linkages to remove the moment would have resulted in the loss of sensitivity in the measurement system, and hence a decrease in accuracy. Nevertheless, actual drag measurements at 48 km/h (6.85 N (1.54 lb$_f$)) compared well to those of an aerodynamic bicycle without a rider (6.23 N (1.4 lb$_f$) from Table 3).

Although this may appear to be a flaw in the vertical mounting system, it was precisely what allowed the drag to be measured with such resolution. By minimizing the amount of structure and linkages between the bicycle and flexure, the losses in the system were kept to a minimum. This "direct" connection to the bicycle allowed slight drag changes to be precisely felt by the flexure. This limitation merely meant that, since the assumed center of pressure didn't vary with fork spacing variations, relative changes in drag must be studied instead of the actual drag values.

4.3.2. Change in Drag Calculation

Changes in drag were determined from the different drag values calculated from the measurements. The drag values were obtained from the following equation:

$$D = \frac{1}{m} \cdot \left(\frac{V_{out}}{E_{in}} - \frac{V_{zero}}{E_{zero}} - b \right) \qquad \text{(Eq. 5)}$$

where m and b are the calibration slope and intercept; V_{out} and E_{in} are the strain gage output and bridge input excitation voltages; V_{zero} and E_{zero} are the zero point (no tunnel air) strain gage

output and bridge input excitation voltages, all respectively. Differences in drag were obtained directly from these values.

4.3.3. Data Correction Factors

The data was corrected for barometric pressure, tunnel temperature, and solid and wake blockages. The solid and wake blockage correction factor (Equation 1) was required because it depends on the drag force, which was not constant. Although a buoyancy correction could have been made for the bicycle data, it was meaningless. Since the correction was constant, it would have applied equally to all of the data and would have been subtracted out during the differencing of the data.

5. Results

Results of the data for various fork spacings are presented in two parts. The first part examines the effect of fork spacing while the last part examines the various effects discussed above. All of the data presented was differenced. The baseline configuration for the differencing was the typical spacing of 2.70 cm (1.0625 in) as indicated in Table 5. All data, unless otherwise stated, was subtracted from the results obtained at the typical fork spacing.

5.1. Fork Spacing

When all of the data at all of the speeds is viewed together (see Figure 25), it is difficult to observe any apparent results other than as speed increases from 40 to 48 km/h and from 48 to 56 km/h, the drag increases by nearly 2 and 4.4 N, respectively. The term "global minimum" in Figure 25 refers to the minimum drag of the baseline spacing at 40 km/h. The vertical line in the figure marks the typical spacing configuration. The close proximity of the multiple data points at

51

each speed and spacing configuration verifies the repeatability of the data. All of the data falls

within the error band (±0.05 N (±0.011 lb$_f$), see Appendix A) of the averaged data. Apparently,
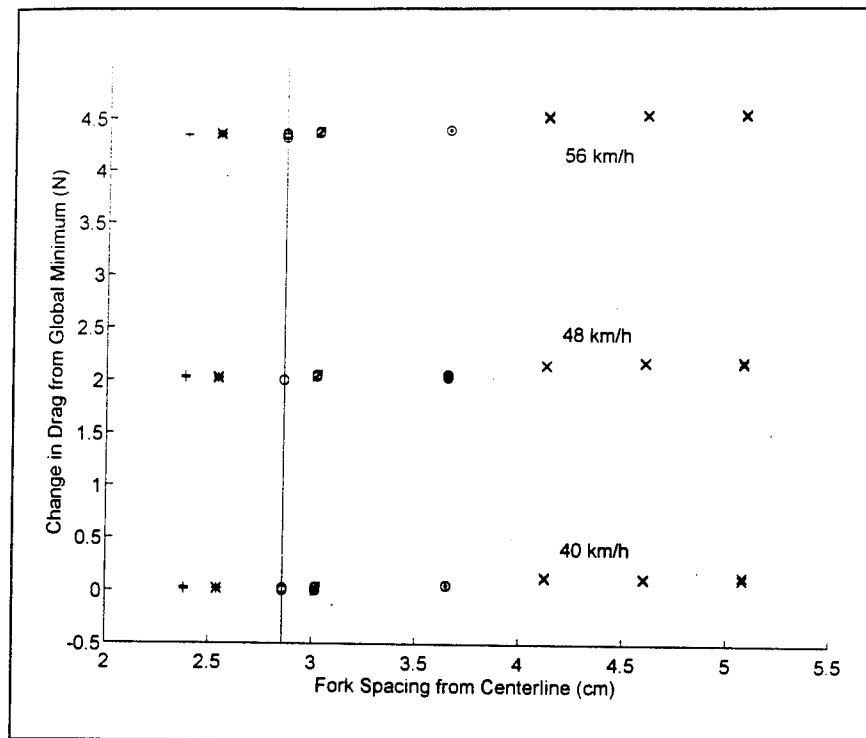
Figure 25. Incremental Drag on a Bicycle with an Adjustable-Width Front Fork Presented at Various Speeds

since the changes in drag are all grouped around the same general value for each speed, the

changes in drag due to fork spacing are minimal.

When the data at each speed is examined separately with respect to the "local minimum,"

the average drag for the baseline spacing at the speed indicated, trends are more easily observed.

Figures 26, 27, and 28 display the data in this manner. Although a best fit curve is not fitted to the

data, the trend at all three speeds are obvious. Narrower fork spacings (2.38 to 3.02 cm) tend to

exhibit a decrease in drag over wider spacings. At 40 km/h. the drag decreases 0.13 N from the widest spacing to the baseline spacing. At 48 km/h. the decrease is 0.20 N. And. the decrease in drag is 0.23 N for 56 km/h. Even when the accuracy of the data is considered. the trend still holds true. Given the trend of the data. it is entirely possible that the drag could continue to decrease at
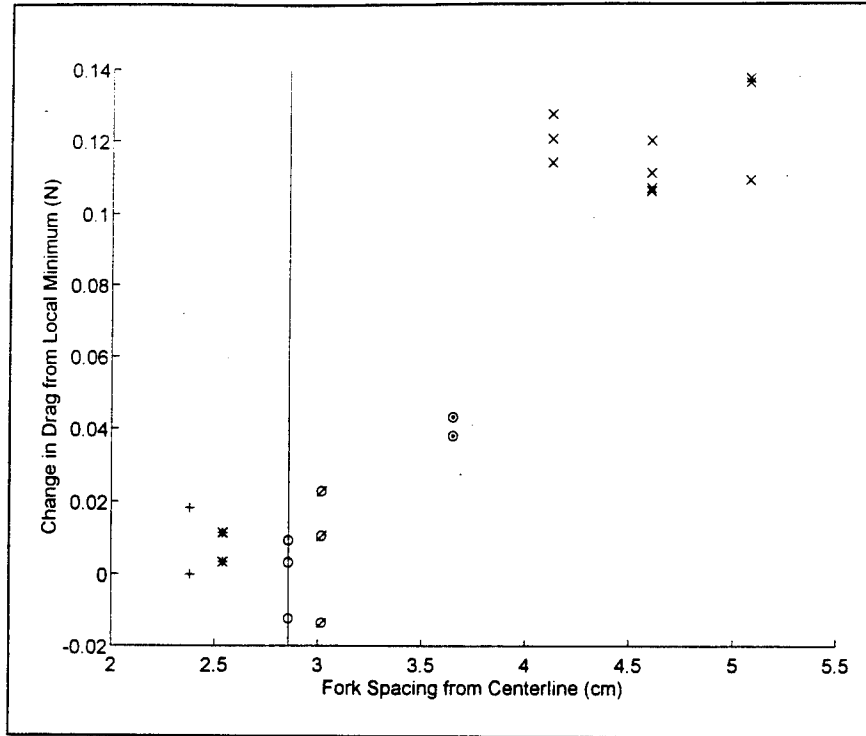
Figure 26. Incremental Drag on a Bicycle with an Adjustable-Width Front Fork Presented at 40 km/h

even narrower spacings than tested. However, it is possible that as the spacing is narrowed even further, the drag will rise as the fork and tire might tend to resemble a large, blunt body.

Table 6 shows the drag changes more precisely in tabulated format. Although it may appear that the only decrease in drag occurs at 56 km/h for a spacing of 2.38 cm, the resolution of the data does not confirm this. All of the changes in drag for configurations with spacing between

Figure 27. Incremental Drag on a Bicycle with an Adjustable-Width Front Fork Presented at 48 km/h

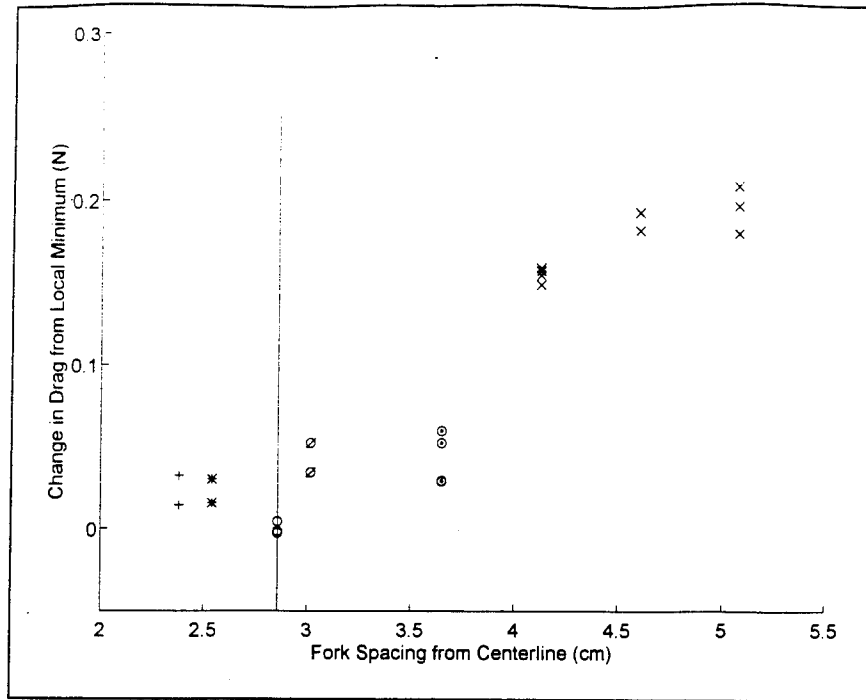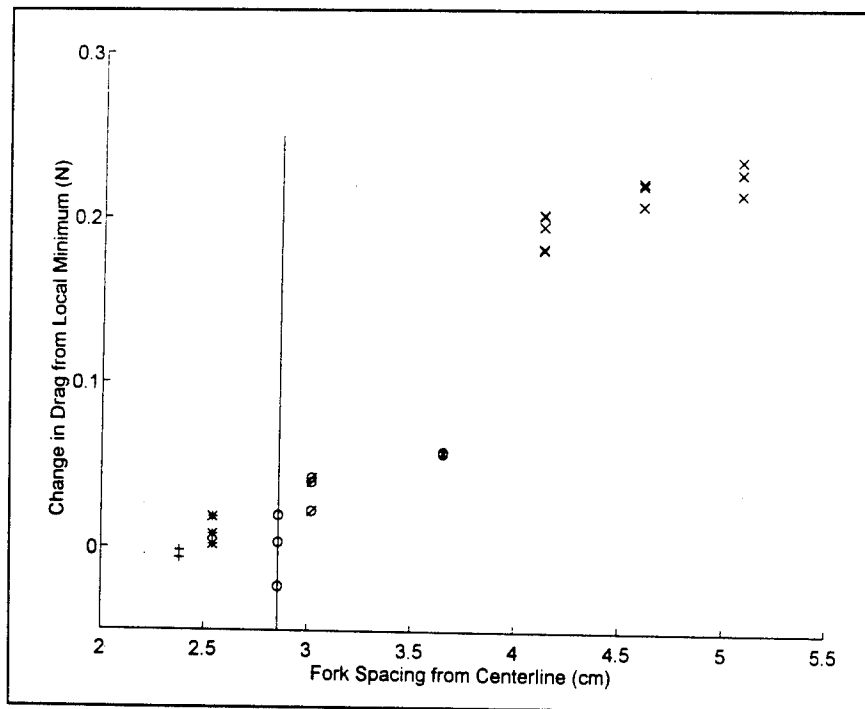**Figure 28. Incremental Drag on a Bicycle with an Adjustable-Width Front Fork Presented at 56 km/h**

2.38 and 3.02 cm for all of the speeds are within the resolution of the measurements. Therefore, no single minimum configuration was found for the minimum drag. Spacings between 2.38 and 3.02 cm can be considered as providing the minimum amount of drag.

Table 6. Average Change in Drag for Spacings at 40, 48, & 56 km/h

Spacing in cm and (in)	Δ Drag @ 40 km/h (N)	Δ Drag @ 48 km/h (N)	Δ Drag @ 56 km/h (N)
2.38 (0.9375)	0.008	0.023	-0.005
2.54 (1.0)	0.007	0.022	0.010
2.86 (1.125) (typ)	0.0	0.0	0.0
3.02 (1.1875)	0.005	0.043	0.035
3.65 (1.4375)	0.040	0.043	0.060
4.13 (1.625)	0.131	0.163	0.197
4.60 (1.8125)	0.112	0.187	0.217
5.08 (2.0)	0.131	0.202	0.229

5.2. Drag of Effects

This section discusses the results of various effects present in the setup. The first effect was that of the spinning wheel. Figure 29 illustrates that the effect of the spinning wheel was minimal (0.04 to 0.08 N), just within the resolution of the data measuring equipment. The combined effect of the air pressure in the air line, the mass flow out the drive unit, and the inertia of the drive wheel was undetectable (0.0 to 0.015 N) as shown in Figure 30. And finally, for the effect of bridging the balance and drag on the drive unit, the drag was observed to be between 0.15 N at 40 km/h and 0.35 N at 56 km/h (see Figure 31). This effect was definitely detectable. The baseline drag for each of the plots was the minimum drag value of the plotted data.
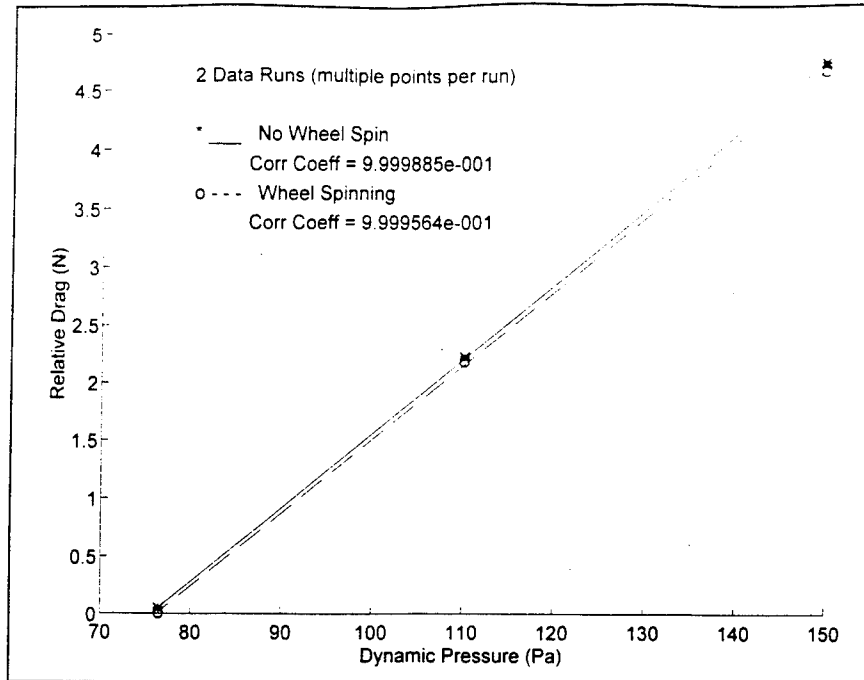
Figure 29. Effect of Spinning Wheel on Change in Bicycle Drag - Comparison of Wheel Spinning and Non-Spinning Runs at Various Dynamic Pressures
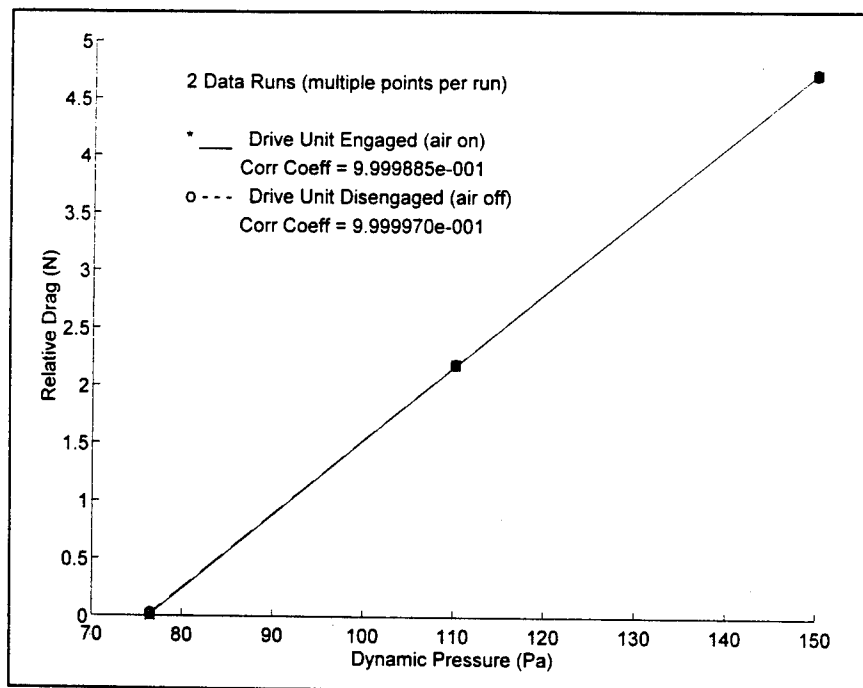
Figure 30. Effect of Air Flow, Mass Flow, and Drive Wheel Inertia on the Bicycle Drag Data - Comparison of Data with Drive Unit Engaged and Not Engaged at Various Dynamic Pressures

If the actual drag values for the bicycle were available, the drag of these effects would have been applied as a correction to the overall drag of the bicycle. However, since the differences in the data were studied, the drag from these effects was immaterial in the analysis.
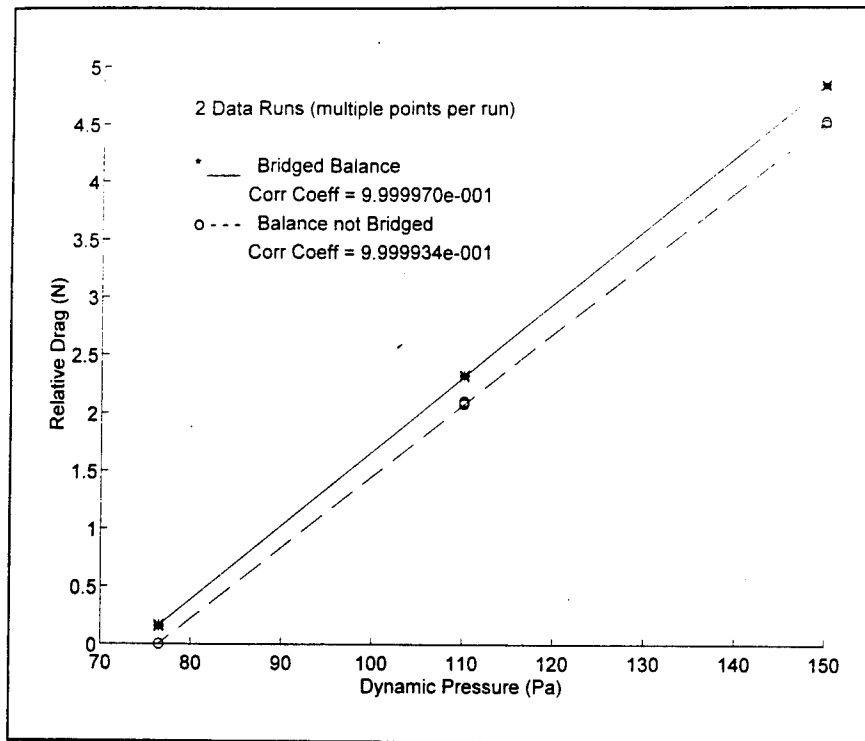
Figure 31. Effect of Bridging the Balance and Drag on the Drive Unit - Comparison of Drive Unit Installed and Not Installed at Various Dynamic Pressures

6. Conclusions and Recommendations

6.1. Conclusions

Without additional data for spacings closer than those tested, it was difficult to make any definite statements on the spacing for the absolute minimum drag. However, one can conclude that a narrower spacing produces less aerodynamic drag than a wider spacing.

Although the data indicated a narrower fork spacing for minimal drag, the typical configuration was already shown to be in the region of minimum drag. Therefore, in terms of aerodynamic drag savings for a bicycle racer, the benefit of additional spacing optimization is minimal. If the racer's bicycle had a wider spacing (3.02 cm and wider), it would be beneficial to reduce the fork spacing by nearly a centimeter. In this case, the benefit of reduced spacing is greater for elite cyclists traveling faster as the savings are greater at higher speeds.

6.2. Recommendations

Several recommendations can be made to enhance the quality of data collected and for continued research on bicycle drag. These recommendations include the elimination of the moment in the vertical sting, examining narrower fork spacings and various configurations, and increasing the realism of the tests.

6.2.1. Moment Elimination

The first recommendation is to eliminate the moment on the vertical sting, or develop a method to determine the center of pressure for the bicycle. If the actual drag values were obtainable, not only would the data have been more valuable, the apparatus would also. In order to compare the results obtained in the tunnel using the vertical system with other sources, actual drag

values were required. Having these values would enhance the credibility of the data in the scientific community.

Two methods to accomplish this are presented. The first is through a modification to the vertical sting. The vertical mounting system could be altered to eliminate the moment arm problem through the installation of a set of linkages between the model and the flexure. A possible set of moment-eliminating linkages could be composed of four bars configured into a parallelogram connected with "frictionless" bearings (see Figure 32). The moment would rotate the linkages and thus become eliminated from the setup. The actual drag would then be measured from the flexure. However, the linkages would reduce the accuracy of the system. Recall that it was this lack of additional linkages that allowed the drag to be measured with such resolution.
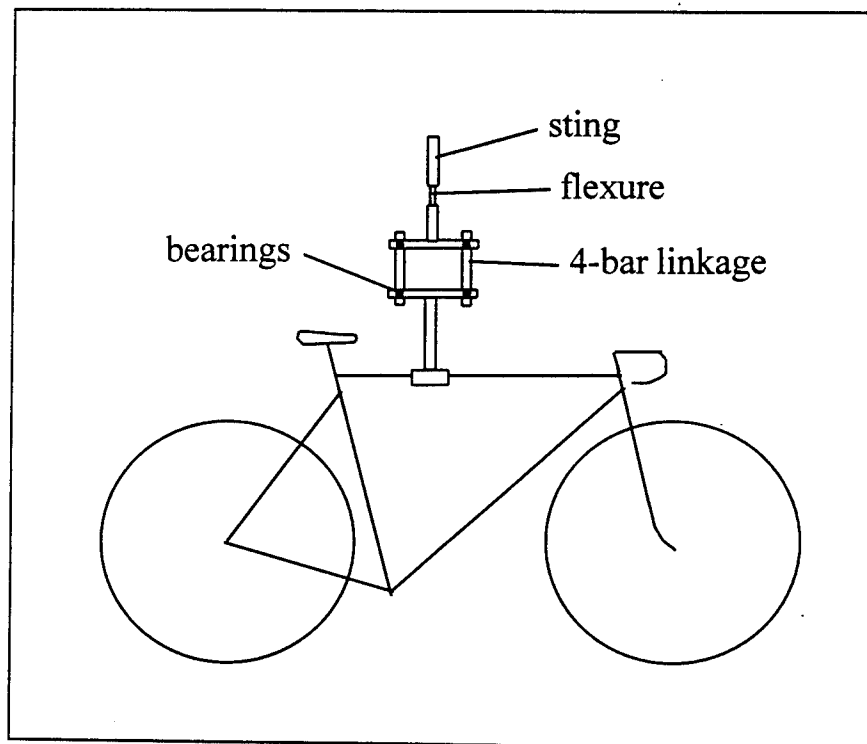

Figure 32. 4-Bar Moment Elimination Configuration

The second method would be through the use of a secondary line used to zero the flexure. A line could be hooked to the front of the bicycle to provide a means of offsetting the drag so that the flexure is returned to its zero value. The pulling force would be measured when the original pre-run zero value was obtained. In this way, the moment arm of the pulling force and the force required to zero the flexure would be known. The force would be the drag of the bicycle. Matching the pre-run zero value may prove difficult due to the oscillations in the system.

6.2.2. Narrower Spacing and Various Configurations

There was nearly 0.48 cm of clearance left between the fork blades and the tire at the minimum spacing used during this experiment. Reducing this spacing could provide additional insight into whether or not narrower spacing would lower the drag farther. In addition, different wheel types and blade shapes could be tested in order to reduce the drag. Also, crosswind effects need to be studied as they are very important. It would take a very small increase in drag due to a crosswind to change a potential drag savings into a drag increase.

6.2.3. Increasing the Realism

As was previously mentioned, the spinning of the wheel was not entirely realistic. During the experiment, the wheel speed corresponded to the velocity of the bicycle. This was an inaccurate representation of the relative velocity of the fork to the top of the wheel. Since this was the primary area of interest as far as drag was concerned, the speed of the wheel at that point should have been the most accurate. Therefore, the wheel spin speeds should have been increased by a factor of two as the top of the wheel travels twice as fast as the bicycle travels. This would lead to a more accurate real-world representation of the flow interaction effects between the fork and tire.

In addition, the ground effect simulation was poor. First, since the ground plane was stationary, it did not realistically represent calm conditions of the real world. In addition, since the bicycle rotated due to the applied moment, the front wheel was positioned relatively far (estimated at 1 cm) from the ground plane in the wind-off condition so that as the bicycle rotated during the tests at the highest speeds, it did not contact the ground. The gap for the rear wheel increased as the tunnel speeds increased. Therefore, the ground plane was viewed as adding little to the realism of the study. It did, however, provide a level surface on which to work.

References

Hoerner, Sighard F. Fluid Dynamic Drag. Published by author, 1965.

Hopkins, Mark W. and Frank S. Principe. "The Du Pont Aerodynamic Bicycle Wheel." Cycling Science: 3-7 (March 1990).

Kita, Joe. "Alcala Wins Ruta Mexico." Bicycling: 16 (April 1994).

Kyle, Chester R. and Edmund Burke. "Improving The Racing Bicycle," Mechanical Engineering: 34-45 (September 1984).

Kyle, Chester, R. "The Aerodynamics of Handlebars & Helmets," Cycling Science: 22-25 (December 1989).

Kyle, Chester R., Ph.D. "Wind Tunnel Tests of Bicycle Wheels & Helmets," Cycling Science: 27-30 (March 1990).

Kyle, Chester R. "New Aero Wheel Tests," Cycling Science: 27-30 (March 1991a).

Kyle, Chester, R. "Ergogenics for Bicycles," in Perspectives in Exercise Science and Sports Medicine, Volume 4: Ergogenics - Enhancements of Performance in Exercise and Sport. Ed. David R. Lamb, Ph.D. and Melvin H. Williams, Ph.D. Wm. C. Brown Publishers, 1991b.

Parker, Brian A. A New Drag Measurement System for Wind Tunnel Testing of the Racing Bicycle and Rider to Determine a Low Drag Configuration. MS thesis, AFIT/GAE/ENY/94D-17. School of Engineering, Air Force Institute of Technology (AU), Wright-Patterson AFB OH, December 1994.

Rae, William H., Jr. and Alan Pope. Low-Speed Wind Tunnel Testing. New York: John Wiley & Sons, 1984.

Swart, Randy. "Hard Facts About Bicycle Helmets," Cycling Science: 14-16 (December 1989).

"Whipping the World," Bicycling: 16 (November 1994).

Appendix A - Error Analysis

There are many ways to determine an overall estimate of error for a given calculation that is based on several measurements. For this study, the error was estimated using the standard error method. This method provides a root sum square most probable error estimate. The error is determined from

$$Error_{RSS} = \sqrt{\left(\Delta u_1 \cdot \frac{\partial s}{\partial u_1}\right)^2 + \left(\Delta u_2 \cdot \frac{\partial s}{\partial u_2}\right)^2 + \ldots} \qquad \text{(Eq. 6)}$$

where Δu_1 is the uncertainty of that particular parameter in the calculation and $\frac{\partial s}{\partial u}$ is the sensitivity of the calculation to that parameter.

The axial force, or drag, was calculated from the reduction formula, Equation 5, repeated here

$$Drag = \frac{1}{m} \cdot \left(\frac{V_{out}}{E_{in}} - \frac{V_{zero}}{E_{zero}} - b\right) \qquad \text{(Eq. 5)}$$

where m and b are the calibration curve slope and intercept; V_{out} and E_{in} are the strain gage output and bridge input excitation voltages; V_{zero} and E_{zero} are the zero point (no tunnel air) strain gage output and bridge input excitation voltages, all respectively. The standard error for the calibration is

$$Error_{force} = \sqrt{\left(\frac{\Delta V_{in}}{m \cdot E_{in}}\right)^2 + \left(\frac{-V_{in} \cdot \Delta E_{in}}{m \cdot E_{in}^2}\right)^2 + \left(\frac{-\Delta V_{zero}}{m \cdot E_{zero}}\right)^2 + \left(\frac{V_{zero} \cdot \Delta E_{zero}}{m \cdot E_{zero}^2}\right)^2} \qquad \text{(Eq. 7)}$$

where the uncertainty quantities are according to Table 7. Note that, the sensitivity and error due to the calibrations slope and intercept are zero since the calibration resulted in correlation coefficients of 0.99999.

Table 7. Component Uncertainties

Component	Uncertainty (V)
ΔV_{in}	48.8×10^{-6}
ΔE_{in}	4.8×10^{-3}
ΔV_{zero}	48.8×10^{-6}
ΔE_{zero}	4.8×10^{-3}

Application of the above to the collected data resulted in the following estimated errors. For the cylinder data collected with the single component balance, the typical error for a data set was estimated at 0.0534 N (0.012 lb$_f$). Similarly, the bicycle data for the single component balance yielded typical errors of 0.0489 N (0.011 lb$_f$). These values compare to static check load results that showed errors of 0.022 N (0.005 lb$_f$). The standard error is thus conservative but also accounts for the uncertainty associated with a dynamic measurement. In addition, these accuracies could be bettered by accounting for the number of data samples collected. However, neglecting this correction in the accuracy also helped to account for the dynamics of the measurements. For the cylinder data collected with the commercial balance, the error was estimated based on the information provided by the manufacturer. In this case, the error was 1% of the full scale load of 222 N (50 lb$_f$) or 2.2 N (0.5 lb$_f$).

Vita

Captain Alan W. Elledge was born on 8 October 1965 in Indianapolis, Indiana. He graduated for Parkway North High School, Creve Coeur, Missouri in 1984 and attended the University of Illinois at Urbana-Champaign, Illinois. He graduated with a Bachelor of Science in Aeronautical/Astronautical Engineering in May 1989. During college and prior to active duty, he worked as a co-op student at McDonnell Douglas in St. Louis, Missouri. As a regular officer, he entered active duty at Wright-Patterson AFB in October 1989 as the Test and Evaluation Director for the Variable Stability In-Flight Simulator Test Aircraft (VISTA) Program. There he remained until entering AFIT in May 1993. His next duty station is Edwards AFB, CA.

Permanent Address: 3224 Nantucket
                                      Springfield, OH 45503

REPORT DOCUMENTATION PAGE

Public reporting burden for this collection of information is estimated to average 1 hour per response, including the time for reviewing instructions, searching existing data sources, gathering and maintaining the data needed, and completing and reviewing the collection of information. Send comments regarding this burden estimate or any other aspect of this collection of information, including suggestions for reducing this burden, to Washington Headquarters Services, Directorate for Information Operations and Reports, 1215 Jefferson Davis Highway, Suite 1204, Arlington, VA 22202-4302, and to the Office of Management and Budget, Paperwork Reduction Project (0704-0188), Washington, DC 20503.

1. AGENCY USE ONLY (Leave blank)	2. REPORT DATE December 1994	3. REPORT TYPE AND DATES COVERED Master's Thesis

4. TITLE AND SUBTITLE
THE DESIGN AND DEVELOPMENT OF A LOW-SPEED, LOW-FORCE WIND TUNNEL DATA ACQUISITION SYSTEM WITH AN APPLICATION TO BICYCLE FRONT FORK SPACING

5. FUNDING NUMBERS

6. AUTHOR(S)

Alan W. Elledge, Captain, USAF

7. PERFORMING ORGANIZATION NAME(S) AND ADDRESS(ES)

Air Force Institute of Technology, WPAFB, OH 45433-6583

8. PERFORMING ORGANIZATION REPORT NUMBER

AFIT/GAE/ENY/94D-21

9. SPONSORING / MONITORING AGENCY NAME(S) AND ADDRESS(ES)

Bruce Campbell
WL/XPT Bldg 45
2130 Eighth St. Ste 1
Wright-Patterson AFB OH 45433-6523

10. SPONSORING / MONITORING AGENCY REPORT NUMBER

11. SUPPLEMENTARY NOTES

12a. DISTRIBUTION / AVAILABILITY STATEMENT

Approved for public release; distribution unlimited

12b. DISTRIBUTION CODE

13. ABSTRACT (Maximum 200 words)

This thesis encompassed the design, development, and application of a low-speed, low-force data acquisition system for the AFIT 5-ft Wind Tunnel. The new data acquisition system was designed and developed to measure approximately 0.045 N (about 0.01 lb$_f$) at nearly 64.4 km/h (40 mph). Verification of the capability was obtained through testing of a cylindrical model. As part of a technology transition program with Wright Laboratory, this new system was used to investigate bicycle front fork blade spacing in order to determine the optimal spacing for minimum drag. As for the minimum drag of a bicycle with an adjustable-width front fork, the spacing should be kept to a minimum.

The wind tunnel was deemed to have sufficiently smooth and steady flow for conducting low-speed research at or above 29 km/h (18 mph), the minimum tunnel velocity using the rear set of motors with the flow straightener positioned directly in front of the inlet.

14. SUBJECT TERMS

wind tunnel tests, aerodynamic drag, drag reductions, vehicles

15. NUMBER OF PAGES
79

16. PRICE CODE

17. SECURITY CLASSIFICATION OF REPORT	18. SECURITY CLASSIFICATION OF THIS PAGE	19. SECURITY CLASSIFICATION OF ABSTRACT	20. LIMITATION OF ABSTRACT
Unclassified	Unclassified	Unclassified	UL